

THREE DIMENSIONAL RADIATION DOSIMETRY
BASED ON OPTICALLY STIMULATED FLUORESCENCE
COMPUTED TOMOGRAPHY OF A NOVEL DNA DOSIMETER

by

RYAN PHILLIP MARCHILDON

A thesis submitted to the
Department of Physics, Engineering Physics & Astronomy
in conformity with the requirements for
the degree of Bachelor of Science, Engineering Physics

Queen's University
Kingston, Ontario, Canada

April 2012

ABSTRACT

A novel form of dosimetry using fluorophore-marked DNA fragments may provide a powerful platform for future high-sensitivity and spatially-resolved dose measurements of all radiation types. This thesis investigates the feasibility of DNA-based 3D fluorescence computed tomography in the context of oncological radiation therapy. A thorough computational model is developed with physical designs for a DNA phantom and readout apparatus. The dose reconstruction algorithm developed is similar to first-generation CT techniques and requires the collection of a fluorescence response for well-defined optical excitations. Numerical simulations indicate a promising agreement between the reconstructed dose profile and the true profile; however, the results generally suffer from systematic inaccuracies due to the spatial dependence of the detector cross-sections. To achieve performance comparable to other dosimetry CT techniques, future work must seek to mathematically correct this confounding phenomenon.

ACKNOWLEDGEMENTS

I would like to thank Dr. Andrew Kerr at the Cancer Centre of Southeastern Ontario for his excellent supervision. Our conversations were always enjoyable and his support helped ensure that this thesis stayed on track during what has been a particularly chaotic year. His feedback on this written report was also of immense help.

I also extend my warm thanks to Tara Wood at the Royal Military College of Canada for her much-appreciated assistance in providing information and clarifications about the DNA dosimetry platform, as well as Dr. Timothy Olding at CCSEO for his expertise in gel and optical dosimetry.

Finally, I would like to thank all of the students and faculty that I have had the great pleasure of working with over the course of my undergraduate degree. My colleagues and instructors have made Engineering Physics a truly incredible experience that has pushed the boundaries of what I am capable of and given me memories that will last a lifetime.

TABLE OF CONTENTS

ABSTRACT.....	i
ACKNOWLEDGEMENTS.....	ii
TABLE OF CONTENTS.....	iii
NOMENCLATURE.....	iv
1. INTRODUCTION.....	1
2. BACKGROUND & THEORY.....	4
2.1 – The DNA Dosimeter.....	4
2.2 – Computed Tomography & the Radon Transform.....	6
3. APPROACH & DESIGN.....	8
3.1 –Literature Review.....	8
3.2 – Proposed Solution.....	8
3.3 – Phantom Design.....	10
3.4 – Excitation Beam.....	11
3.5 – Detector Selection & Electronics.....	12
3.6 – Final Design.....	20
4. SIMULATION & NUMERICAL MODEL.....	26
5. POST-PROCESSING OPTIMIZATION & RESULTS.....	31
6. CONCLUSIONS & RECOMMENDATIONS.....	36
7. REFERENCES.....	37
8. APPENDICES.....	40

NOMENCLATURE

<u>Symbol</u>	<u>Definition</u>
h	Plank's Constant [$6.626 \cdot 10^{-34}$ m ² kg/s]
c	speed of light in vacuum [299,792,458 m/s]
N _A	Avogadro's Number [$6.022 \cdot 10^{23}$ mol ⁻¹]
λ	wavelength [m]
t	time [s]
A	cross-sectional area [m ²]
Q	quantum efficiency
[C]	concentration [mol/L]
I	intensity [W/m ²]
σ	absorption cross/section [cm ²]
μ	linear attenuation coefficient [cm ⁻¹]
M	linear coefficient for dose vs. broken DNA [$2.7 \cdot 10^{-3}$ μM/Gy at [C] = 0.5 μM]

Acronyms

DNA	Deoxyribonucleic Acid
SSB	Single-Strand Breaks
FAM	Fluorescein Amidite Molecules
BHQ	“Black Hole Quencher” [Molecules]
PMT	Photomultiplier Tube
CCD	Charge-coupled Device
RMC	Royal Military College (of Canada)
LINAC	Linear Accelerator (Radiation Therapy Platform)

CT	Computed Tomography
MRI	Magnetic Resonance Imaging
FRET	Förster's Resonance Energy Transfer
(wt)	"By Weight"
3D	Three-Dimensional
PETE	polyethylene teraphthalate
ADC	Analog-to-Digital Converter
APD	Avalanche Photodiode
DFT	Discrete Fourier Transform

Miscellaneous

Voxel	A cubical unit of finite resolution – the 3D analogue of a pixel
Gray (Gy)	SI unit for absorbed radiation dose: 1 Gy = 1 Joule radiation/1 kg matter

1. INTRODUCTION

Radiation therapy, an essential component of cancer treatment, relies on the careful application of high-energy photons to kill cancerous cells at the tumour site while minimizing the dose absorbed by surrounding healthy tissues [1]. Oncological radiation treatment has evolved over the past several decades into a sophisticated, technology-driven process in which all aspects of dose planning and delivery are electronically controlled.

Modern medical linear accelerators (LINACs), as depicted below in Figure 1, represent the state-of-the-art in patient care [2]. Accelerated electrons are collided with a tungsten filament inside the machine head, producing a beam of high-energy X-rays through a bremsstrahlung process [3]. This X-ray beam is then conditioned by a complex array of collimators, providing control over the beam topology [2]. A gantry allows the LINAC head to rotate 360 degrees around the patient, enabling the target site to be accessed from multiple angles. This combination of beam shaping and dose angle – along with the ability to modulate beam intensity – facilitates unprecedented optimization of dose delivery such that the damage to healthy tissue is minimized [2,3].

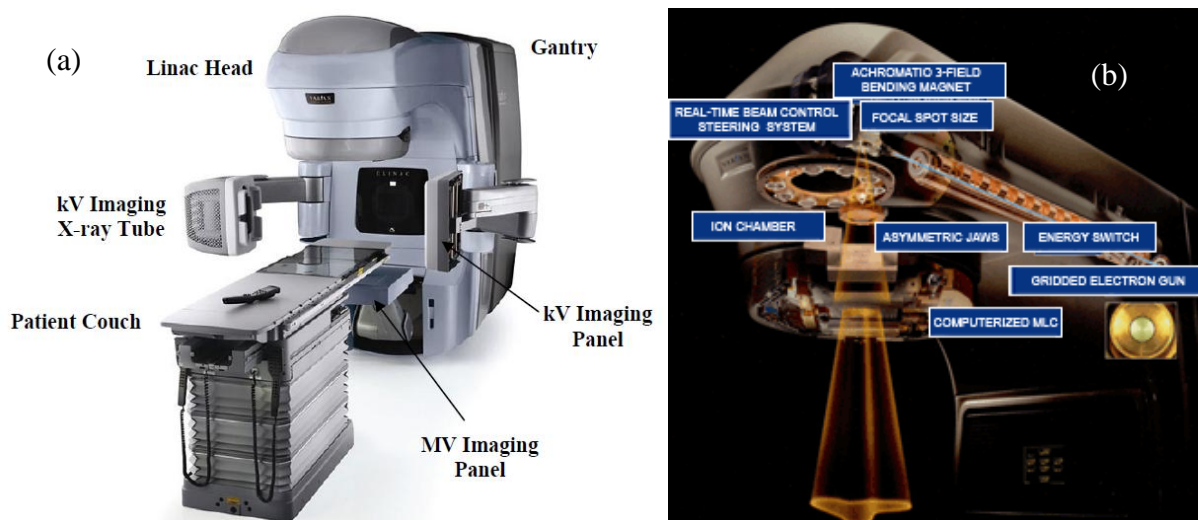


Figure 1 – A modern LINAC for radiation therapy (a), and details of LINAC-based beam creation and conditioning (b). [4]

Patient-specific treatment plans are typically created with computer assistance, using images of the tumour site acquired through x-ray computed tomography (CT). The treatment process is a highly sophisticated endeavour, owing to the complexity of dose delivery and the number of programmable degrees of freedom. Comparison between actual dose delivery and planned dose delivery is therefore a necessary measure of quality assurance [2,5]. A common practice is to first test treatment plans on non-living targets, thereby allowing dose discrepancies to be identified and corrected. Such targets are colloquially referred to as ‘phantoms’. The phantoms typically contain materials that are susceptible to radiation-induced changes in their local optical properties [5]. Information about the delivered dose profile can then be extracted by a readout system employing conventional CT techniques. The acquisition of dose data from an irradiated structure is known as ‘dosimetry’.

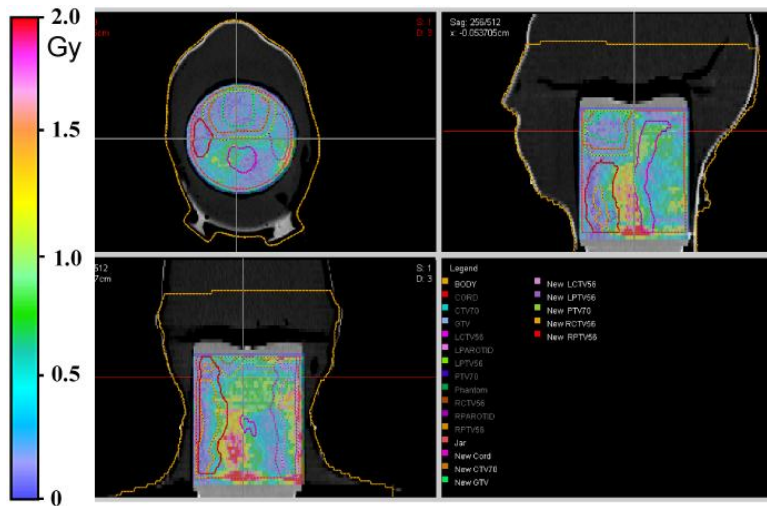


Figure 2 – Example depicting the use of a jar-shaped phantom for aiding oncological LINAC-based radiation treatment planning. This phantom has been placed within a head-shaped vessel that helps emulate the effect of surrounding tissues. [5]

This thesis seeks to investigate the feasibility of creating a 3D dosimetry platform (i.e. phantoms and an accompanying readout system) using a novel form of dose detection based on the radiation-induced fragmentation of DNA strands. Such a system must be capable of resolving both the magnitude and the spatial distribution of the delivered dose – a feat that has not previously been explored for a DNA-based platform. Given that performance will depend heavily on the underlying photochemistry, optics, and reconstruction algorithms, strong

emphasis is placed on the creation of a thorough computational model as a proof (or disproof) of the concept. Apparatus designs will support the simulation development and provide complementary information about anticipated costs, scanning time, and limitations in the physical implementation.

DESIGN OBJECTIVES:

In the context of clinical use, the most important design considerations are accuracy and reliability as well as the safety of the user. Dosimetry platforms used for medical quality-assurance purposes are assessed with criteria known as the “gamma map” [6]. To pass this test, more than 95% of the reconstruction voxels must match either the true dose intensity to within 3% (in the case of low dose gradients) or the true spatial dose profile to within 3 mm (in the case of high dose gradients) [6]. Existing dosimeters are usually able to offer spatial resolutions of 2 mm or less, with some systems achieving accuracies to well within 1 mm [2]. Given this, it would be reasonable to aim for a spatial resolution of 2 mm with a DNA-based system. During a session of radiation therapy, local dose levels typically range between one and two Grays. A Gray (Gy) is the SI unit for absorbed radiation dose, and is defined as the absorption of one Joule of ionizing radiation by one kilogram of matter (i.e. tissue) [2]. At the very least, a DNA dosimeter system should aim for a dose resolution of 0.05 Gy or better, permitting the dose scale to be quantized to at least 40 distinct states.

Secondary design considerations* are ease of operation and scan time. Financial cost is also a significant consideration and will be analysed; however, it is not given the same level of importance as other design criteria for two reasons: 1) in the healthcare market, performance advantages tend to be more heavily weighted than cost; 2) the system’s novel nature will make it more expensive than established alternatives a-priori.

* A discussion of “social” or “environmental” factors is not applicable to this thesis topic in the usual sense, and therefore do not appear (there would be little to talk about, if anything).

2. BACKGROUND & THEORY

2.1 - The DNA Dosimeter

The term “dosimeter” broadly refers to any device that measures absorbed radiation dose through the interaction of incoming high-energy photons with a detection medium (i.e. a gas, gel or semiconductor) [7]. In practice these devices range from simple ‘proportional’ counters for monitoring occupational exposures, to spatially-resolved configurations such as those used in radiation treatment planning. A research group at the Royal Military College of Canada (RMC) has recently developed a novel dosimetry technique in which DNA serves as the detector [7].

Short strands of DNA are augmented on either end by molecules with specific functionalities. The first of these is a fluorescein amidite molecule (FAM) that emits a fluorescence signal when optically excited. The spectral properties of this ‘fluorophore’ are shown in Figure 3 below.

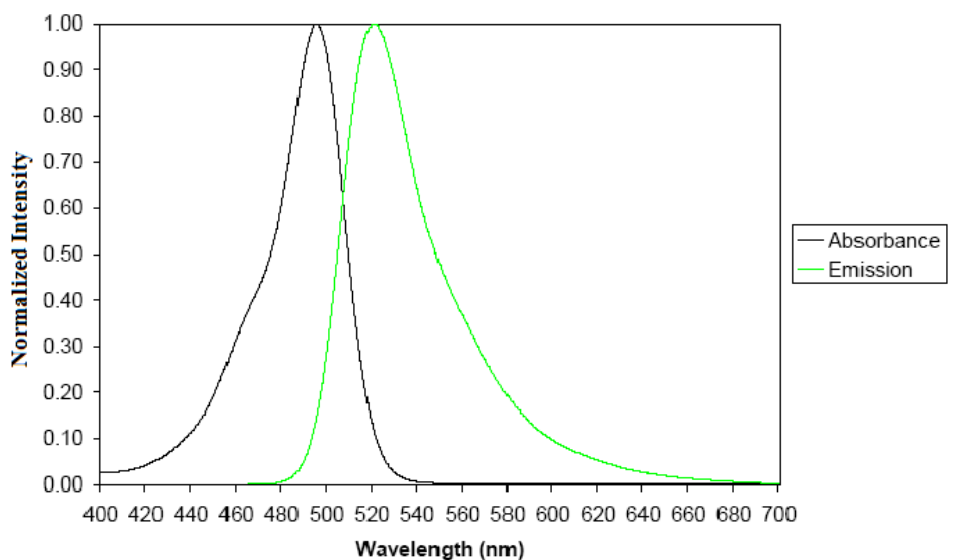


Figure 3 – Absorption and Emission characteristics of the FAM used in DNA dosimetry [8]. The difference between the absorbed and emitted wavelengths is known as the Stokes Shift.

Attached to the opposite end of the DNA strand is a molecule known as a Black Hole Quencher (BHQ). This molecule couples to the FAM through an electric dipole interaction that suppresses the FAM fluorescence signal through a phenomenon known as Förster's Resonance Energy Transfer (FRET) [7,9]. The probability of FRET scales inversely with the sixth power of distance, much like the Van der Waals force.

A 'single strand break' (SSB) occurs when a DNA strand is severed by radiation or radiation by-products such as free radicals [10]. With nothing anchoring them together, the two halves of the strand drift apart due to entropy effects, spatially separating the BHQ and FAM molecules such that the probability of FRET is greatly decreased. In this manner, a SSB is able to release a detectable fluorescence signal indicating that it has suffered radiation damage [7].

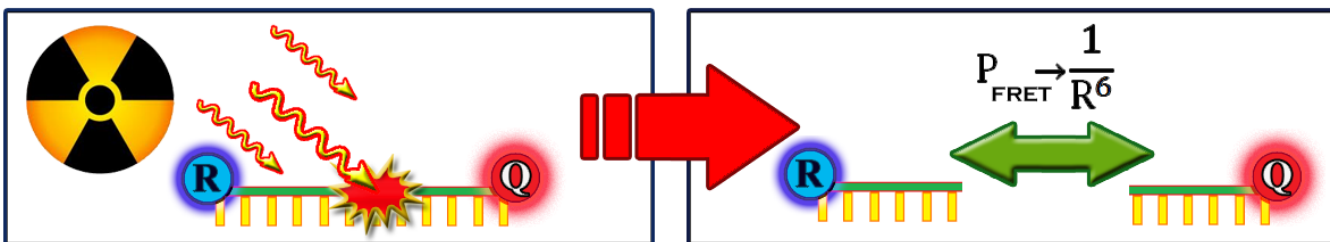


Figure 4 – Illustration of the dosimetry mechanism. Unbroken DNA fragments are labelled with an optically-active, fluorescing 'reporter' molecule and a fluorescence-absorbing 'quencher'. An electric dipole interaction (FRET) prevents the release of a fluorescence signal. When the DNA fragment is severed by radiation, the two ends drift apart due to entropy and the probability of FRET decays as $1/R^6$, enabling a detectable fluorescence response.

DNA is of particular interest as a dose-detecting medium due to its responsiveness to a wide variety of radiation types (i.e. other than ionizing radiation) as well as its clear correlation with biological damage [7]. The experimental group at the RMC found a linear relationship between the number of detected SSBs and the radiation dose that produced them, which makes it easy to relate changes in fluorescence response to relative changes in delivered dose [7,8,10]. Finally, experimental results indicated that the DNA may have unsurpassed sensitivity compared to other existing dosimetry mediums. Before investigating the feasibility of extracting dose information from irradiated DNA-based phantoms, it is first necessary to review the underlying principles behind CT reconstruction.

2.2 – Computed Tomography & the Radon Transform

At optical frequencies, photon attenuation is primarily attributable to Rayleigh scattering and photoelectric absorption [11]. For a beam of photons, the cumulative effects of all possible attenuation processes can be collectively encapsulated by a single linear attenuation coefficient ‘ μ ’. If a beam with an initial intensity of I_0 travels a distance ‘ x ’ through a material with an attenuation coefficient ‘ μ ’, then the final intensity of the beam is given by the Beer-Lambert law:

$$I(x) = I_0 e^{-\mu x} \quad [12]$$

Computed tomography (CT) techniques have traditionally taken advantage of the fact that the total attenuation of a beam projected through an object with locally-varying attenuation coefficients is given by the following line integral:

$$\frac{I}{I_0} = e^{-\int \mu(r) dr}$$

where “ r ” is a spatial coordinate [11,12].

In 1917, Johann Radon conceived of a compact mathematical representation of an image in terms of line integrals over a set of straight lines “ L ”:

$$R(L) = -\ln\left(\frac{I}{I_0}\right) = \int_L \mu(r) dr$$

This is known as the Radon transform, and implies that it is possible to mathematically find a function $\mu(r)$ that satisfies this relation for a known set of attenuated projections [11,12]. In other words, since $\mu(r)$ usually depends on material density and type, it is possible to reconstruct a cross-sectional image of an object from nothing more than attenuation measurements.

One way of determining $\mu(r)$ is through the use of the Fourier Slice Theorem. This theorem states that the Fourier Transform of $R(L)$ at a specific projection angle yields a unique line in the frequency domain of the full 2-dimensional image [12]. Due to the linearity of the Fourier Transform, the frequency data from multiple projection angles can be used to sample the entire 2D frequency domain, which can then be transformed back to the spatial domain to yield a fully-reconstructed image [11,12]. This concept is illustrated in Figure 5.

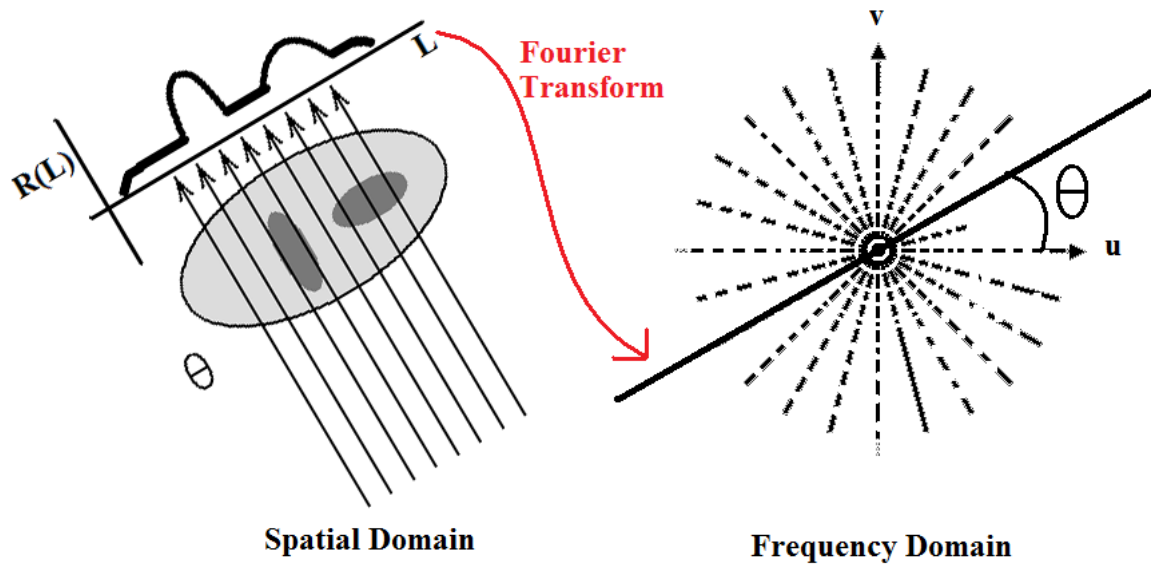


Figure 5 – Illustration of the Fourier Slice Theorem. The Fourier Transform of the projection data through an object at a specific angle yields a unique line in the 2D Fourier Transform of the total object. Attenuation data at multiple angular increments can thus be used to sample the total frequency space, which can then be subjected to an inverse Fourier Transform to yield a reconstructed cross-sectional image of the object. Note that projections at angles beyond 180° begin to produce gratuitous results in the frequency domain.

The Fourier Slice Theorem is the backbone of CT techniques. One common implementation is known as the ‘back-projection’, whereby the object is numerically divided into finite elements (pixels for a 2D slice and voxels for a 3D object). Attenuation data from multiple angles is then superimposed upon this grid and begins to resemble the object cross-section as the sampling resolution increases [11,12].

3. APPROACH & DESIGN

3.1 –Literature Review

Background research was conducted into existing fluorescence and dosimetry CT techniques to gain useful insight into how potential solutions might be approached. A multitude of different methodologies were examined, the details of which are available elsewhere [13-16]. In brief, many of these schemes used stochastic analyses relying on Monte Carlo methods or a computationally-intensive “Boltzmann Transport Equation”.

Techniques in optical dosimetry were also examined, due to their widespread use in radiation therapy. Optical dosimeters are often formed of gelatine structures laced with radiation-responsive monomers [5]. Dose delivery stimulates a polymerization processes (due to initiation by free-radicals) that turns the gel optically opaque. The dose distribution can then be extracted by a form of standard CT that uses a cone-shaped beam instead of linear projections (thereby permitting faster readouts) [5].

Although effective in their specific applications, most of the surveyed methodologies are not amenable to a DNA-based platform. Reconstruction techniques based on the Boltzmann Transport equation require the specimen to be highly-scattering (i.e. a tissue), whereas this is not a valid assumption for a DNA dosimeter [16]. Furthermore, schemes based on Monte-Carlo reconstructions would require a robust way of determining signal origin and would lead to a highly complex apparatus and computational algorithm. Finally, cone-beam CT is only possible when attenuation is being measured (as opposed to a fluorescence response) [14]. Extracting information from a DNA dosimeter therefore requires a unique solution; albeit one that takes inspiration from existing techniques.

3.2 – Proposed Solution

If a well-defined excitation beam is passed through a DNA dosimeter, then the resultant fluorescence signal will be directly proportional to the total radiation dose within the beam path.

Furthermore, if the beam shape is rectilinear, then a modified first-generation CT algorithm based on the Fourier Slice Theorem can reconstruct the dose distribution from increases in emitted fluorescence signal (rather than decreases in beam signal due to attenuation). This concept is illustrated in Figure 6. Full 3D reconstruction would be done on a slice-by-slice basis along the length of the dosimeter, requiring a set of linear excitations through the phantom at angular orientations from 0° to 180° for each slice. Such a readout device requires a ‘stable’ phantom, geometric simplicity, the capacity to rotate or translate the phantom, an appropriate detector array, and excellent control of the excitation beam.

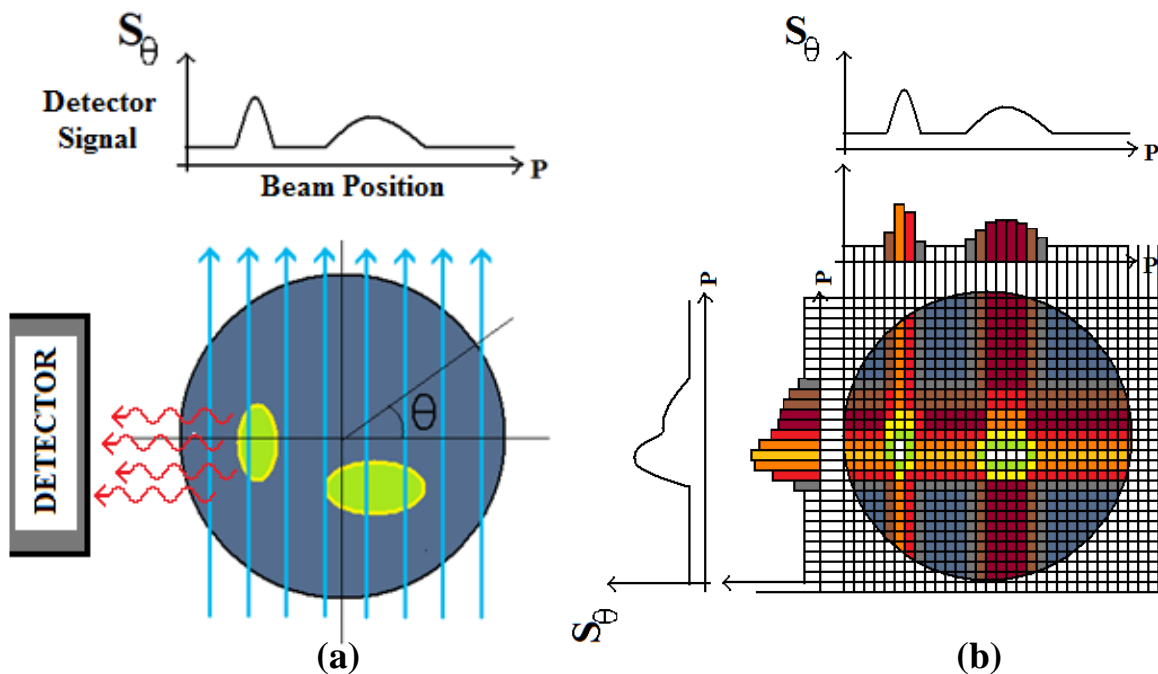


Figure 6 – (a) A series of fluorescence measurements are taken as a linear excitation beam is translated across the phantom. (b) The data obtained from multiple orientation angles is then combined to reconstruct the dose distribution via the Radon Transform/Fourier Slice Theorem. [Note: the Green ellipses within the phantom indicate an irradiated area.]

It is important to note two additional differences between the proposed solution and traditional attenuation-based CT. Since the fluorescence response is assumed to be emanating from SSB sources as a spherical flux of photons, the total fraction of this flux reaching the detectors will depend on the relative position of the sources. Secondly, there will be additional attenuation of the fluorescence signal as it propagates towards the detectors; this is also a

position-dependent phenomenon. The severity of the two effects will be investigated through simulation.

3.3 – Phantom Design

Since phantoms designed for optical dosimetry are already in clinical use, it is reasonable to base the DNA phantom on existing practices. The phantoms employed in optical CT are comprised of a gelatine or colloidal suspension matrix laced with low levels of radiosensitive chemical species [17]. Colloidal suspension is achieved using a 30% silica-in-water solution. Once radiosensitive molecules have been added, a change in the pH or water content can cause the silicon to ‘self-attract’ and effectively freeze-up the solution. Gelatine suspension is achieved using a collagen-derived protein that forms a three dimensional matrix at room temperatures [17]. The gel liquefies above a certain transition temperature, permitting it to be homogenously mixed with additives.

To decide between the two techniques, it is important to consider how the DNA dose sensitivity and fluorophore response are impacted by environmental factors. FAM quantum efficiencies as well as ionized free-radical production (and therefore DNA damage) have a significant dependence on solution pH [10]. Since silica solutions are known to suffer from pH instabilities, gelatine – which always has a pH of 7 – is the favourable choice.

Gelatine also allows for easy and reliable preparation. The gel is heated up to 50 degrees Celsius to liquefy, and then is slowly allowed to return to room temperature. DNA can be added when the temperature reaches 32° C (i.e. normal internal body temperature), since the protein matrix does not begin to reform until roughly 28°C and below [17].

Completing the phantom design requires a choice of gelatine concentration, DNA concentration, and phantom shape. A 5% (by weight) solution of gelatine-in-water provides enough structure to ensure the DNA fragments remain spatially stable [17]. Higher gelatine concentrations would lead to unnecessary signal attenuation as well as undesirable changes in refractive index. DNA concentration must be chosen to balance signal size with response linearity. As DNA concentration increases, there is a higher probability of FAM-labelled SSB

fragments drifting too close to BHQ molecules and undergoing FRET, thereby confounding the linear dose vs. detected SSB relationship [7]. A DNA concentration of 0.5 μ M was recommended by the experimental group at the RMC [8,10]. Finally, the shape of the phantom was chosen to be an 8cm-diameter, 10cm-deep cylinder contained in a thin-walled polyethylene terephthalate (PETE) jar. This choice was made to emulate the optical CT phantom designs as closely as possible [5].

3.4 – Excitation Beam

SOURCE & SHAPE:

A 488 nm Argon-based laser would serve as an efficient excitation source since the FAM absorption peak sits at approximately 490 nm as shown in Figure 3. This source must be capable of pulsing the beam at a rate of up to 100 Hz (see discussion below). Beam size must be chosen based on an appropriate compromise between signal level, dose resolution and scanning time (see Section 3.6) – to this end, a beam width of 2 mm was selected. Using this beam size, an 8cm-diameter phantom slice could be reconstructed using an angular step-size of 2 degrees and a planar step size of 2 mm, requiring a total of $(80\text{mm}/2\text{mm}) \cdot (180^\circ/2^\circ) = (40) \cdot (90) = 3600$ measurements. Since reconstruction algorithms typically break the phantom into cubical voxels, it is preferable that the beam has a square cross-section as opposed to a circular one. Both cross-sectional size and shape are easily conditioned through the use of an optical aperture.

INTENSITY & DURATION:

Ideally, the intensity of the beam would be made as high as possible to maximize the measurable fluorescence response; however, a phenomenon known as photobleaching limits the amount of excitation light that can be used. Photobleaching refers to the self-destruction of excited fluorophores through chemical reactions with their environment, and is a probabilistic process. Hence, there is a statistical limit to the number of times a fixed quantity of fluorophores can be excited before significant degradation of their signal response occurs. Experimental results from the RMC indicate that signal degradation due to photobleaching should be

negligible (i.e. less than 2%) provided that fewer than 10^{13} excitation photons are used during slice reconstruction [18]. For a 2mm-wide beam at 488 nm, this is equivalent to 3600 pulses at 100 mW and 28 ms in duration.

A second constraint on beam intensity comes from photodetector saturation, which poses a problem that is most pronounced when extremely sensitive devices are required. Unlike photobleaching, this does not necessarily mean that the total number of excitations must be limited. Rather, signal saturation can be prevented by spreading out the excitations over a longer period of time, i.e. decreasing the beam intensity and increasing the pulse duration. A more detailed discussion can be found in Section 3.5.

PATH CONTROL:

Accurate reconstruction requires that the beam path through the phantom is well-controlled. An obvious complication with a cylindrical phantom is that refraction can occur as the beam enters the dosimeter jar, making it difficult to achieve the desired excitations. The easiest solution is to surround the phantom in an ‘index-matching’ tank, as is common practice in optical CT [5]. In such a setup, the excitation beam enters the tank at normal incidence and traverses a fluid with a refractive index matching the index of the phantom.

The index of refraction at 488 nm for a 5% (wt) gelatine-in-water solution is approximately $n_{\text{gel}} = 1.345$. A 10-12% (wt) propylene glycol-water mix would achieve an identical refractive index with minimal attenuation [5]. The PETE jar has a refractive index of $n_{\text{jar}} = 1.575$. Thus, provided that the dosimeter PETE jar is kept extremely thin, the excitation beam would experience negligible bending as it passed from the tank fluid into the phantom and out again, regardless of the angle at which it hits the dosimeter jar.

3.5 – Detector Selection & Electronics

Many different photodetector technologies exist on the market, with an immense variety of applications. Some of the most common devices are described below:

Photodiodes are comprised of n-type and p-type semiconductor layers that are biased to form a depletion region [19]. If an impinging photon possesses energy greater than the diode's semiconductor band-gap, its absorption will produce an electron-hole pair that is subsequently turned into a photocurrent by the depletion region's built-in electric field [19]. Photodiodes benefit from high quantum efficiencies, good linearity, and low costs, but have small areas and are generally unable to resolve low light levels (i.e. hundreds of photons). Better sensitivity can be achieved using avalanche photodiodes (APDs), but at a significant increase in cost.

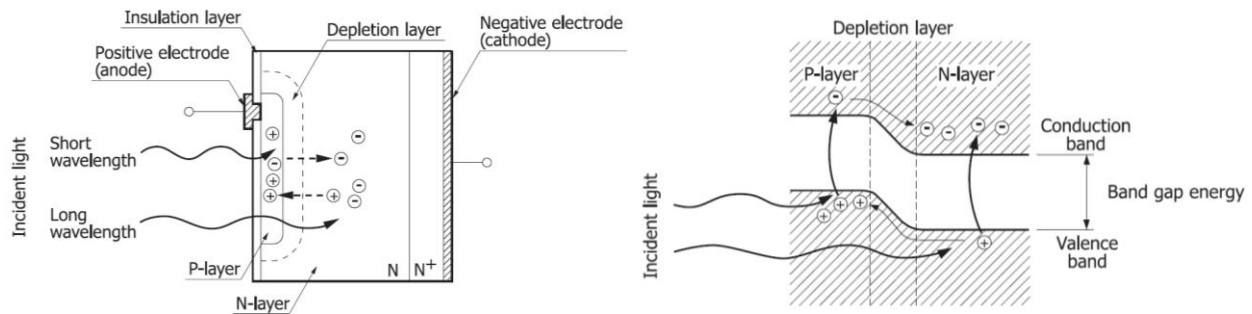


Figure 7 – Illustration of photodiode operation depicting device construction (left) and the semiconductor band structure (right). [19]

Charge-coupled devices (CCDs) are arrays of semiconductor pixels that accumulate a photoelectron charge upon illumination [20]. These charges can be multiplexed through voltage amplifiers to readout electronics. CCDs thus behave as an electronic camera, with a spatial resolution of up to 1.1 μm and typical quantum efficiencies of 70%. Low-light applications typically employ fast gating and thermoelectric cooling [20]. Due to their small size, CCDs often require optical focusing.

Photomultiplier tubes (PMTs) achieve detection through the photoelectric effect, whereby impinging photons eject electrons from a photocathode material [21]. These photoelectrons then enter a cascade of high-voltage dynodes, producing an avalanche effect capable of amplifying the initial photocurrent by 6 to 12 orders of magnitude. PMTs are thus best-suited for applications involving low-intensity (or even single-photon) signals.

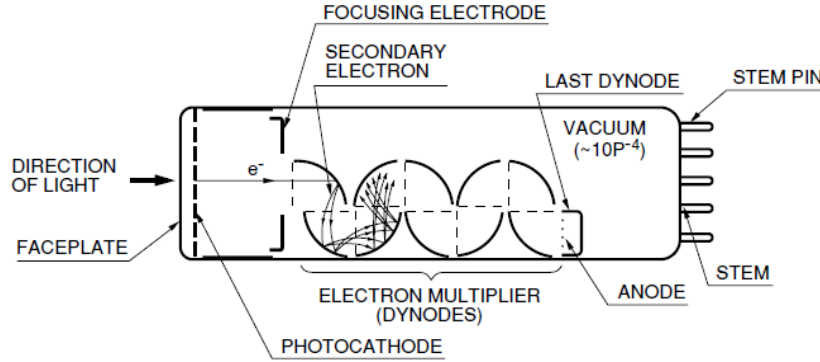


Figure 8 – Schematic showing the basic features of a PMT. [21]

ESTIMATING THE SIGNAL LEVEL:

The optimal choice of photodetector type is largely dependent on anticipated signal levels. A preliminary calculation of the fluorescence response is therefore a necessary first-step in narrowing down the number of feasible options.

Typical dose-readout experiments conducted by Wood and colleagues at the RMC employ a 10-watt pulsed excitation beam that is active for a total of 16 μs over a 16 ms period [8,10,18]. Using these parameters and the equations found in Section 4 for a 2 mm^3 voxel and an excitation wavelength of 488 nm, an estimated 74,386 fluorescence photons will be re-emitted from an excited voxel per Gray of absorbed radiation. Assuming that these photons are emitted as a uniform spherical flux and that they do not undergo significant attenuation, only $\sim 15\%$ will reach an intermediately-sized detector surface (i.e. for a detector cross-section of $9\pi \text{ cm}^2$ placed 5 cm axially from the source). Therefore, to achieve the desired dose resolution of 0.05 Gy, the chosen detection system must be capable of creating a distinct signal from roughly 300 to 600 impinging photons that arrive over a 16 ms span.

Based on the above discussion, photomultiplier tubes are best-suited to this task due to their single-photon sensitivities, low noise levels, and relatively large detecting surfaces. High sensitivity avalanche photodiodes or CCD cameras would suffer from decreased signal levels due to their small cross-sections, which is further exacerbated by their significantly higher noise floors. Since the fluorescence response is uncollimated, no satisfactory optical setup could be

conceived that would allow a significant fluorescence signal to be focused onto the active areas of either device.

Furthermore, a price comparison indicates that there is no real cost advantage to using APDs or CCDs as opposed to PMTs. Hitachi offers a 1.69 cm² fluorescence microscopy CCD module with high sensitivity at a cost of \$1000 to \$1500 [22]. APDs with an active area of 0.5 cm² and satisfactory sensitivity specifications are listed by DigiKey at prices approaching \$1000 [23]. For comparison, single PMTs without any auxiliary electronics are typically listed at around \$500, and can have active areas between 20 cm² and 95 cm² [21].

The high voltages (1500-2000 V) required for PMT operation require special safety precautions. To minimize the potential for accidental contact, protective covers will be installed over all live high voltage components to electrically isolate them from the user.

SELECTING A PMT:

PMT performance is largely dependent on the choice of photocathode material, which determines the sensitivity, quantum efficiency, and linearity of the detector as a function of wavelength [21]. Photocathode materials are typically categorized into families of response curves, such as those shown for transmission and reflection mode PMTs in Figures 9 and 10 below. Although the FAM emission spectrum is peaked at 520 nm, its width is spread out between 500 and 600 nm. It is therefore desirable that the PMT response curve be both high and flat in this region. A flat response helps ensure that all detected photons produce equal output signals; however, response curvature and statistical variations can be accounted for with proper calibration. From Figures 9 and 10, the most desirable characteristics correspond to the 555U, 650S and 502K curve types. 555U and 502K employ multi-alkali photocathodes, whereas 650S uses GaAs(Cs). Although reflection-mode curves possess more desirable characteristics, they are typically only found in the 'side-on' variation of PMT in which the optical window is the side of a cylinder rather than a flat circle [21]. Thus the 555U and 650S curves generally do not meet the geometry requirements of the reconstruction scheme.

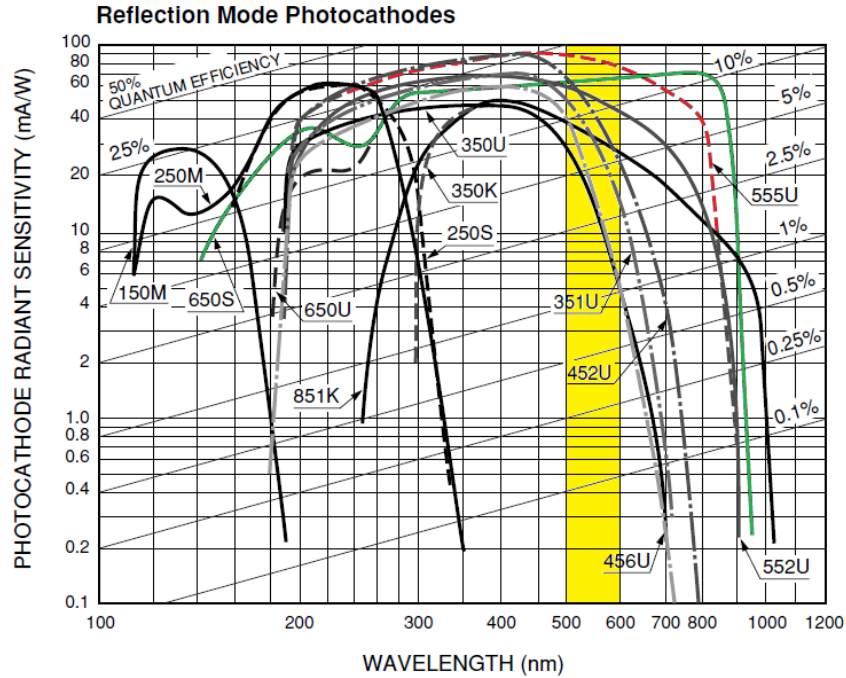


Figure 9 – Wavelength characteristics of reflection-mode photocathodes. The bandwidth of interest has been highlighted, and the curves of the top two performers have been coloured green and red. [21]

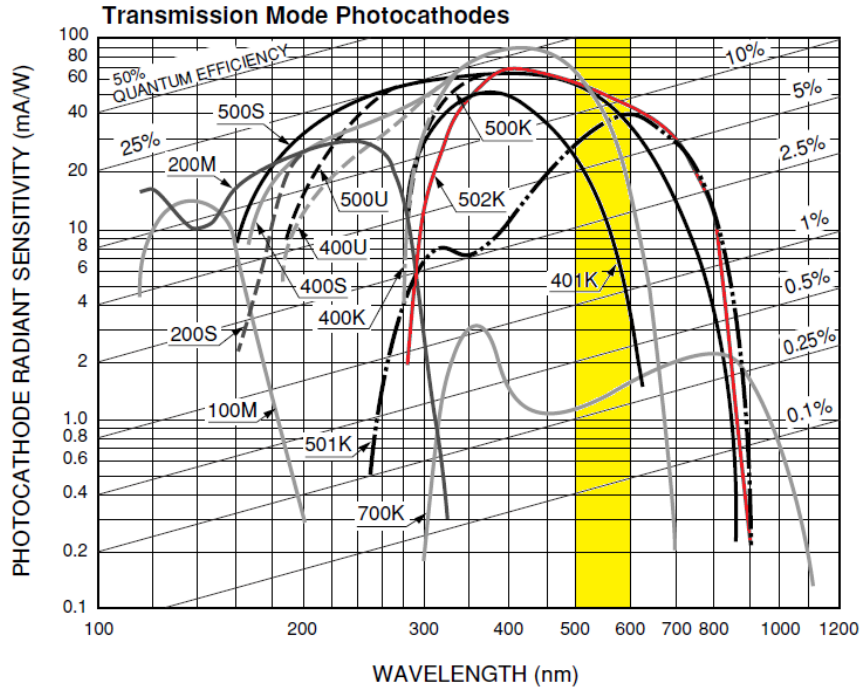


Figure 10 – Wavelength characteristics of transmission-mode photocathodes. The bandwidth of interest has been highlighted, and the curve of the top performer has been coloured red. [21]

Using the response curves as a starting point, a search of the product catalogue of PMT manufacturer *Hamamatsu* yields two potential candidates [24,25]. Table1 compares the specifications of both tubes.

Table 1 – Comparison of key characteristics between two PMT candidates
(averaged between 500 nm and 600 nm)

Product Name	<u>Hamamatsu R943-02</u>	<u>Hamamatsu R1513</u>
<i>Photocathode Material</i>	<i>GaAs(Cs)</i>	<i>Multialkali</i>
<i>Detector Diameter</i>	<i>51 mm</i>	<i>127 mm</i>
<i>Quantum Efficiency</i>	<i>~15%</i>	<i>~10%</i>
<i>Radiant Sensitivity (mA/W)</i>	<i>70 maximum, 60 minimum ($\Delta=10$)</i>	<i>55 maximum, 30 minimum ($\Delta=25$)</i>
<i>Current Gain</i>	<i>$5.5 \cdot 10^5$</i>	<i>$3.3 \cdot 10^5$</i>
<i>Max cathode current (nA)</i>	<i>1</i>	<i>0.3</i>

As inferred from Table 1, the large cross-section of the R1513 PMT more than compensates for its lower quantum efficiency, but it is inferior to the R943-02 in terms of response linearity and maximum cathode current. Generally a lower max cathode current would require the laser excitation pulses to be of lower intensity and greater duration, which can significantly increase the total reconstruction time. However, if the excitation pulses are 100 mW and 28 ms (see section 3.6) then neither PMT is saturated and both are therefore viable candidates. A computer-based numerical simulation would provide a clearer assessment of which option is preferable. In the meantime, the R943-02 will be considered the PMT of choice.

ELECTRONICS MODULES:

High PMT gain and good sensitivity are not enough to ensure that the minimum dose resolution is measurable. Obtaining output levels manageable by an analog-to-digital converter (ADC) requires the use of auxiliary electronics. Assuming that each excitation pulse is at 100 mW and is 28 ms in duration, the system must be designed to resolve a minimum of 500 incident photons (i.e. representing the desired 0.05 Gy dose resolution threshold for a single voxel) as

well as a maximum of 800 000 photons (i.e. representing a beam cutting through the entire diameter of a phantom that has been uniformly dosed with 2 Gy). In general, this can be achieved by employing either a photon counting system (Figure 11) or an integrating charge amplifier (Figure 12).

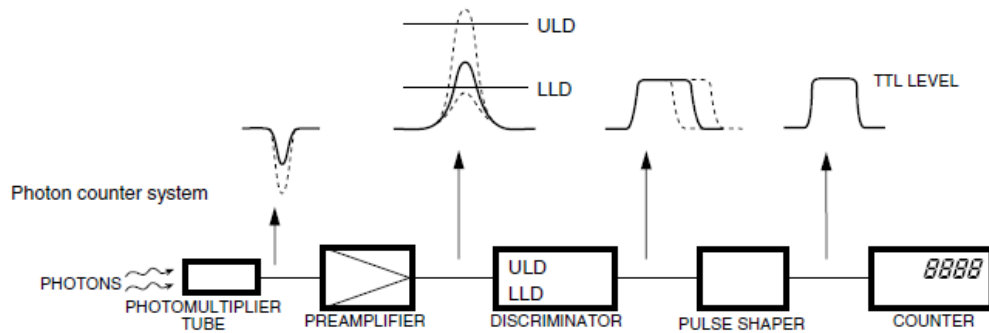


Figure 11 – Overview of a standard PMT photon-counting system. [26]

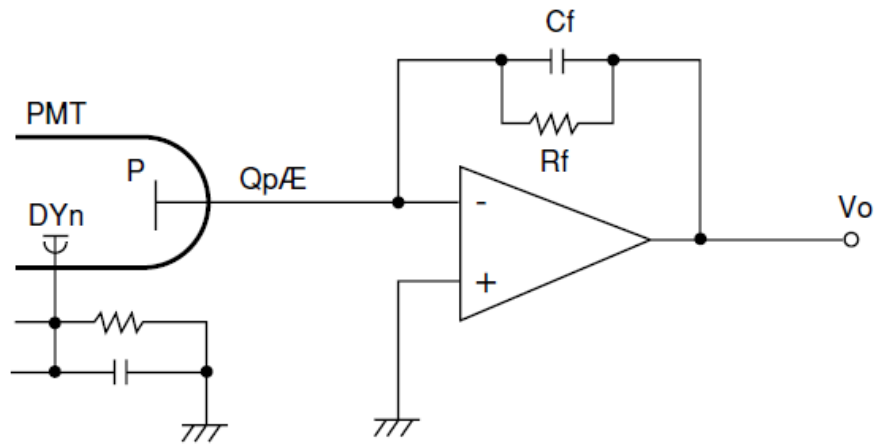


Figure 12 – Simplified schematic of an integrating charge amplifier. The magnitude of the voltage response is set by the capacitance C_f . The larger the time constant $\tau = C_f R_f$, the more the output pulse will resemble Q_p/C_f . [21]

A charge amplifier is the favoured option due to its relative simplicity and reduced cost. For a pulse of charge Q_p emerging from the PMT anode, the impulse response of this circuit is given by the following relation [21]:

$$|V_{out}| = \left| \frac{Q_p}{C_f} e^{-\frac{t}{\tau}} \right|$$

where $\tau = C_f R_f \equiv$ time constant

Provided the time constant is made to be quite large, then the amplifier output will begin to resemble the total accumulated charge divided by the capacitance C_f . This output can be sent through an additional amplifier and into a triggered sample-and-hold circuit for an ADC. To prevent overlap between excitation pulses, the accumulated charge can then be shunted with a switched circuit employing a much smaller time constant. With a PMT having a quantum efficiency of 0.15 and a gain of 5×10^5 (such as the Hamamatsu R943-02), a 1 nF capacitance would produce the following voltage outputs:

For the minimum signal (~500 photons):

$$|V_{out}| = \frac{(e_{charge})(gain)(N_{photoelectrons})}{C_f} = \frac{(1.6 \times 10^{-19})(5 \times 10^5)(0.15 \times 500)}{(1 \times 10^{-9})} = 0.006 \text{ V}$$

For the maximum signal (~800,000 photons):

$$|V_{out}| = \frac{(1.6 \times 10^{-19})(5 \times 10^5)(0.15 \times 800000)}{(1 \times 10^{-9})} = 9.6 \text{ V}$$

This is easily resolvable with a 16-bit ADC (since by distributing $2^{16} = 65,536$ states between 10 V and 0 V, the quantization unit is 0.000153 V),

It is also good practice to gate the PMT to prevent excess light levels from degrading its performance (i.e. such as when the PMT is exposed to background light during the insertion/removal of a phantom). This can be done with an external circuit that reverse-biases the photocathode with respect to the dynode array, preventing any electrons from reaching the amplifier cascade [21]. The bias is then removed by a gate pulse that allows the PMT to operate normally during the pulse duration. The gating signal can have a pulse width as small as 100 ns and a frequency as high as 10 kHz [27].

PMT manufacturers often supply electronics packages with built-in functionalities that include circuits such as those described above as well as a high-voltage power supply. For example, the Hamamatsu H11526-20-NF series module would be perfect for this application except for the fact that the active PMT area is too small [27]. Such modules can cost anywhere between \$2000 and \$3000.

OTHER CONSIDERATIONS:

Any scattering of the excitation beam into the PMTs will saturate the fluorescence measurements, due to the high sensitivities involved. Due to the fact that fluorescence lifetimes are typically between 1 and 10 nanoseconds, it would be infeasible to eliminate potential laser scatter through electronic gating, even if the total excitation energy was condensed into an extremely short pulse. It is therefore necessary to use passive thin-film filters to completely eliminate the 488 nm excitation light.

Such functionality can be achieved using a “496 nm blocking edge Brightline Long-pass filter” available from *Semrock* (part # FF01-496/LP-25) [28]. This filter allows wavelengths of 500 nm and greater to pass through with more than 98% transmission, while blocking wavelengths below 496 nm (transmission < 0.001%). A 32 mm² filter costs \$483, but customized sizes are available. Obtaining a custom-made 50 mm² filter for a R943-02 PMT would cost an estimated \$1000.

3.6 – Final Design

LAYOUT & MECHANICS:

The physical design of the readout system evolved through many stages of revision. An early approach sought to use CCD arrays to capture additional spatial information – at the time it was thought that the spatial resolution of the CCDs could be used to correct any geometric discrepancies entering the CT reconstruction. This initial concept is displayed in Figure 13.

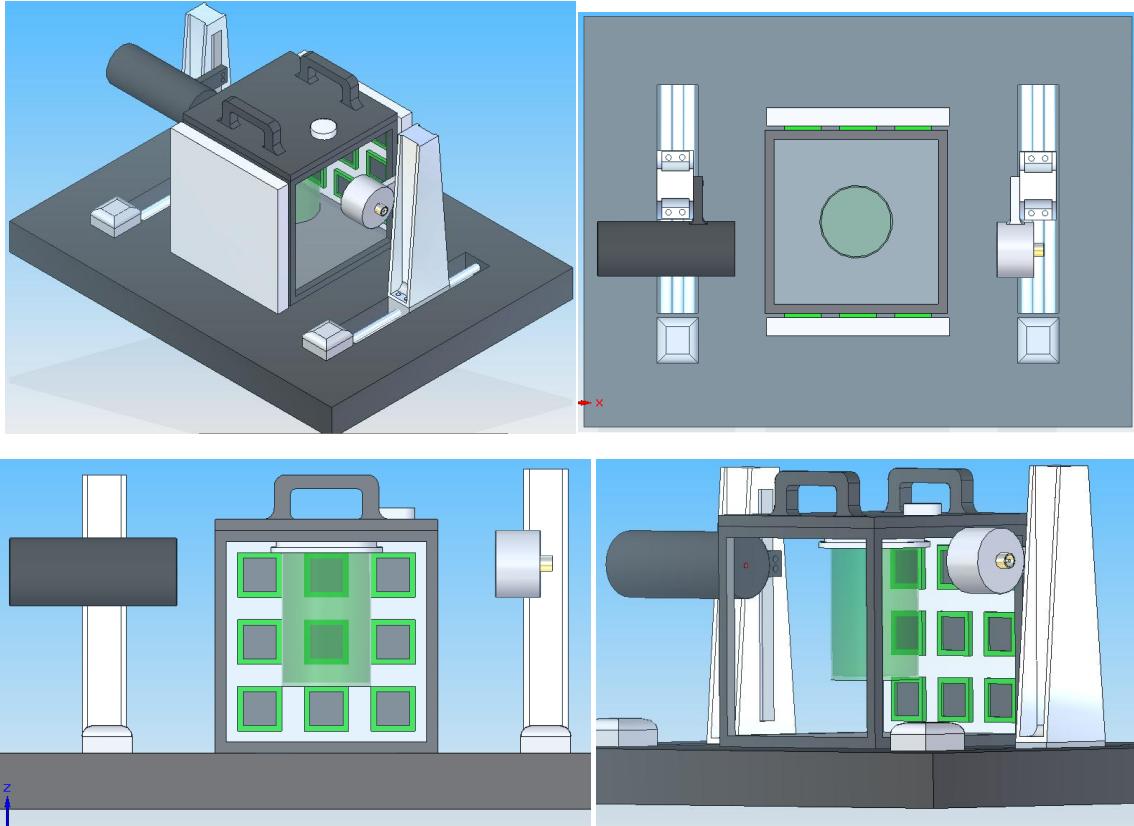


Figure 13 – Views of an earlier concept that employed CCD arrays and also permitted the measurement of beam attenuation as part of a calibration procedure. In this abandoned model, the excitation laser was given two degrees of freedom, and the phantom only moved during rotation. The final design is shown in Figures 14-16.

Eventually, an approach was formulated to establish as much geometric symmetry as possible about the slice plane of interest, making the system easier to computationally model. As is emphasized in Figure 18 (Section 4), the use of two PMTs provides greater cross-sectional symmetry than a single detector. To avoid complications brought on by refraction, the detectors and optical filters are placed as flat against the tank as possible. The tank was made more compact to maximize the cross-sections of the PMTs with respect to sources of fluorescence.

There are several ways of implementing the three degrees of freedom required by a 3D CT scan. For cost and reliability, the most desirable option is one with a minimum of moving

parts and the highest level of simplicity. The rotational degree of freedom can be achieved by using a servo-motor attached to the bottom of the tank lid which clamps around the phantom jar. This is seen in many readout systems for optical dosimetry [5]. The excitation beam can be panned across the phantom using a small 90° mirror mounted on a miniature track, as detailed in Figures 14 through 16. This allows the laser source to remain stationary. Lastly, the ability to vertically shift between phantom ‘slices’ can be accomplished by mounting the matching tank onto a movable, servo-driven platform.

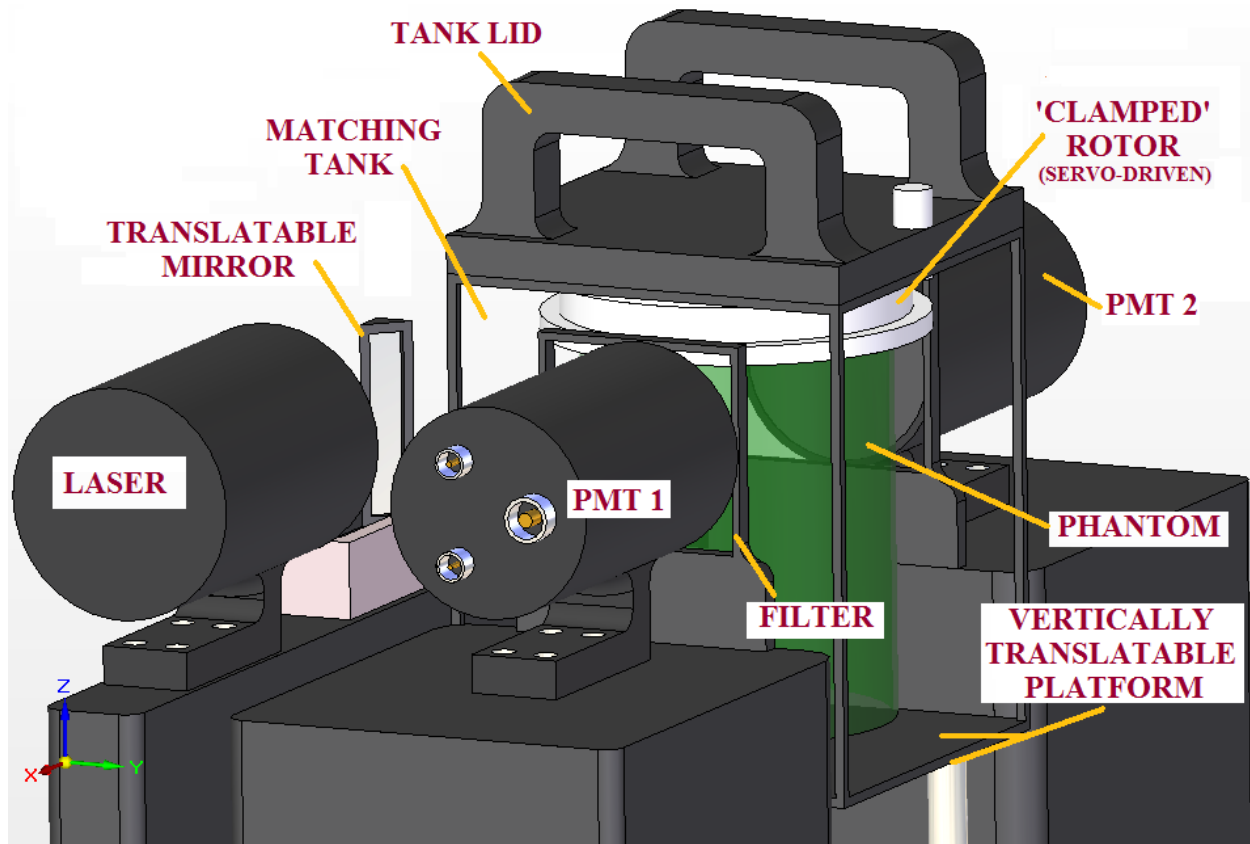


Figure 14 – Functional details of the proposed readout apparatus. The dosimeter jar has been artificially tinted green for visual contrast. A rotating clamp matched to the dimensions of the phantom jar is attached to the bottom of a removable lid. The tank is filled with an index-matching solution of propylene glycol and water. Thin optical filters are placed immediately in front of the PMTs to prevent signal contamination from scattered laser light. Additional views are depicted in Figures 15 and 16.

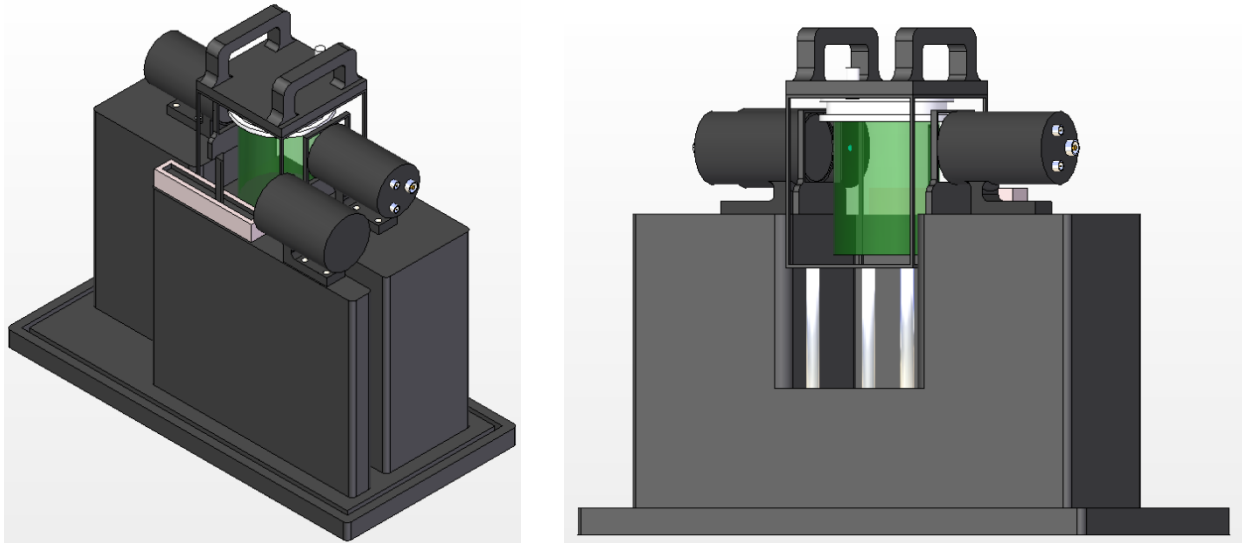


Figure 15 – The final physical layout of the proposed DNA dosimetry readout system. The image on the left shows a view from the front, while the image on the right depicts a view from behind the apparatus. Prior to operation, an opaque case is fit into the base from above, to protect the measurement system from light contamination and to prevent accidental exposure to laser radiation. The base of the apparatus measures 44 cm x 22 cm in dimension.

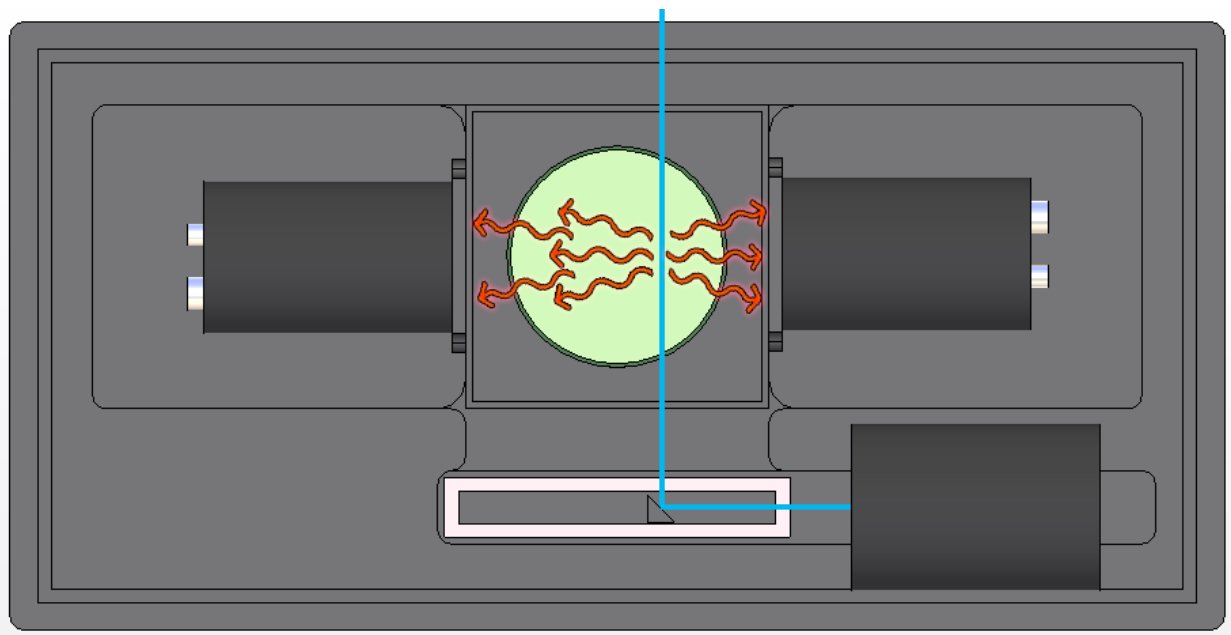


Figure 16 – Top-down view of the apparatus depicting a measurement in action. The tank lid has been removed to show the fluorescence response. The mirror pans left and right to translate the beam across the phantom. Note that in normal operation the apparatus would be covered in an opaque case that fits into the groove around the base periphery.

OPERATION:

A control system is required to ensure proper coordination between degrees of freedom (i.e. phantom rotation, mirror translation), excitation pulses, and sensor gating. Precise timing is critical due to the short excitation times (100 mW for 28 ms). These excitation parameters were chosen to maximize the total fluorescence signal while keeping the total scan time as short as reasonably possible.

One envisioned mode of operation is depicted in Figure 17 below. The mirror translates continuously while the laser beam is pulsed for a 28 ms period every 56 ms*. This requires a total of 2240 ms for each angle. For a total of 90 angular increments, the total time to scan a single slice is 3.36 minutes. Consequently, scanning a full 10 cm long phantom requires $(100 \text{ mm}/2\text{mm}) \times (3.36 \text{ minutes/slice}) = 168 \text{ minutes} = 2.8 \text{ hours}$.

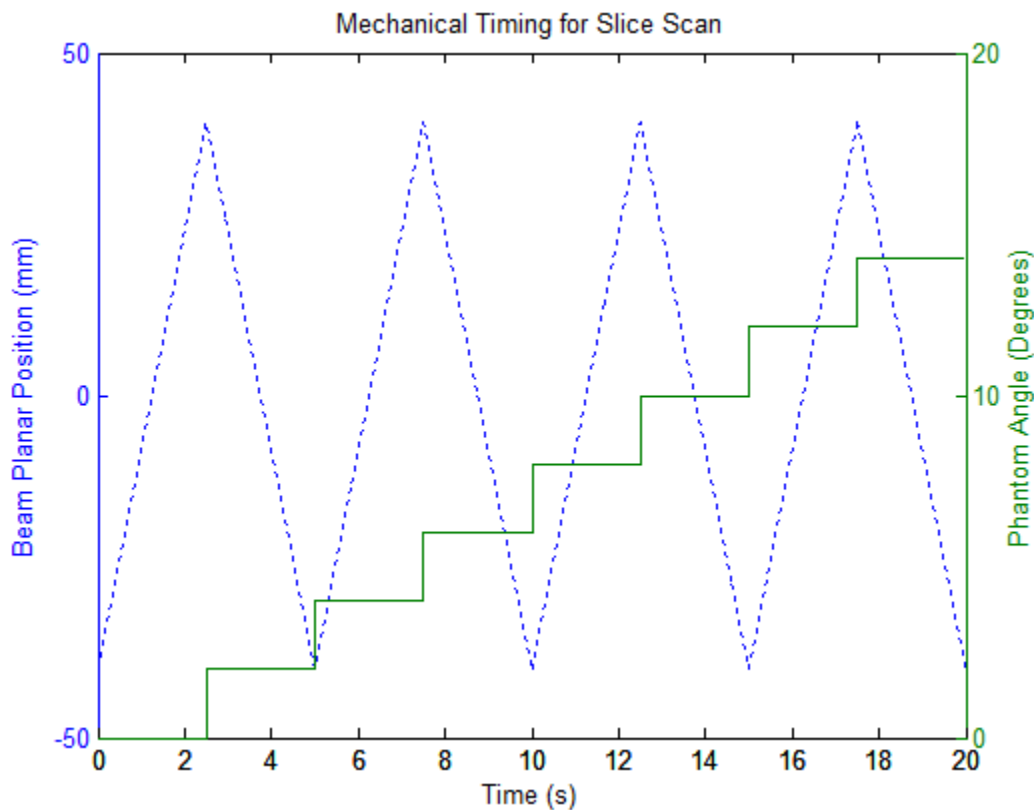


Figure 17 – Graphical display of the coordination between beam position and phantom angle during a slice scan.

* Note the numerical simulation will differ from this in that it resembles a saw-tooth function; the scan always starts on the same side of the phantom.

ESTIMATED COST-BREAKDOWN:

Being a novel technology, the dual-labelled DNA fragments that serve as the dosimetry mechanism are fairly expensive. The supplier, *Biosearch Technologies*, sells the material at a cost of \$365 per micromole [30]. Since each phantom is roughly 0.5 L in volume and contains a DNA concentration of 0.5 μ M, a total of 0.25 μ mol is required per phantom. Allotting \$10 for the PETE jar, each phantom will thus cost roughly \$100. This price expected to decrease within the next several years.

The anticipated costs involved in creating a readout apparatus are shown in Table 2, based on rough quotations available from product suppliers [24,25,27,30,31].

Table 2 – Anticipated Cost Breakdown for DNA Dosimeter Readout Apparatus

ITEM/COMPONENT	ESTIMATED COST
2 <i>Hamamatsu</i> PMTs + Electronics Modules	\$5000
2 <i>Semrock</i> Optical Filters (FF01-496/LP-25)	\$2000
Programmable Logic Controller	\$400
16-bit ADC	\$120
Readout Assembly (Platform & Servos)	\$3000
TOTAL	\$10520

Note: The Argon laser source has not been included; potential prices range from \$1000 to \$10000 [32].

4. SIMULATION & NUMERICAL MODEL

A MATLAB-based simulation package was designed to emulate the physical dosimeter readout as realistically as possible, focusing on a single 2D slice of a 3D phantom. Such a computational model is pivotal in establishing the feasibility of the proposed solution, and also serves as a basis for conducting quantitative evaluations of different design parameters (such as PMT model, beam intensity, etc). The code includes the option of viewing the simulated reconstruction process in real-time. A brief description of each simulation module follows.

NOTE: Recorded examples of the simulator in action can be found at the following URL:

<http://www.youtube.com/watch?v=1FHVSZGmbks>

Video Title: "Computed Tomography with a DNA Phantom"

GRID CONSTRUCTION:

Inputted dose distribution patterns are automatically truncated to fit the dosimeter jar size, and are subsequently mapped to a finite-element (FE) grid. By default, the generated grid size automatically matches the resolution of the dose image (albeit the reconstruction resolution is still determined by the excitation beam width).

CREATION OF LOOK-UP TABLES:

In advance of the simulation, the following geometry-dependent quantities are numerically calculated at periodic locations along the FE grid:

1. Detector cross-section – this will determine the fraction of fluoresced SSB photons that can reach either photodetector from the site of emission. Due to the geometry of the apparatus and detectors, this can be achieved by computing the solid angle subtended by the circular PMT faces [33]. The spatial variance of detector cross-section will have an impact on the reconstruction quality.

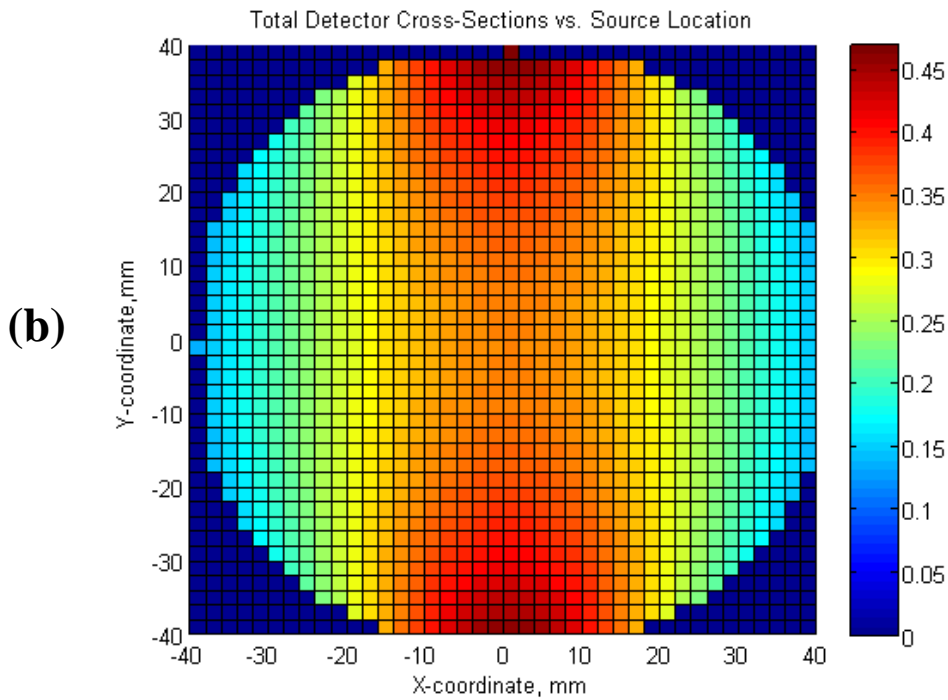
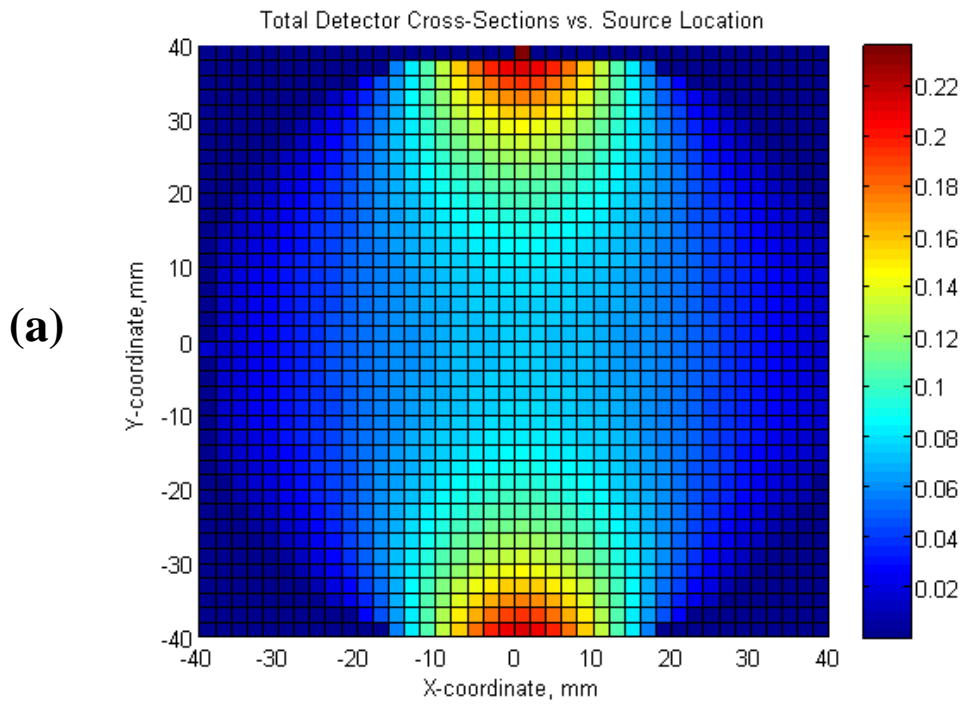


Figure 18 – Combined detector cross-sections as a function of fluorescence source for (a) the R943-02 PMT [51 mm diameter] and (b) the R1513 PMT [127 mm diameter]. The scale used represents the fraction of generated photons that can reach the detectors based on geometry considerations alone (not taking attenuation into account).

2. Average path length through phantom – this allows an average signal attenuation to be determined. The computation is again made possible by the apparatus geometry, and is achieved by integrating over all paths from the point of emission to the detector's projection onto the phantom jar and then dividing by the area of integration.
3. Average path length through matching tank – this is similar to #2, but follows from the subtraction of #2 from the average path length to the detector.

Since every FE voxel at any angular orientation can be mapped to a particular spot in the detectors' reference frame, the use of pre-calculated lookup tables reduces the simulation's total computational time by more than a factor of fifty.

GENERATION OF EXCITATION BEAM:

Laser excitation is simulated in the reference frame of a stationary phantom – thus the beam pans and rotates across the FE grid according to the specified angular and translational step-sizes. For each coordinate in the Radon Transform (i.e. $F(\theta,s)$), the beam determines which of the FE voxels have been 'excited'.

Note: It was originally thought that beam attenuation would also be measured; thus, this algorithm keeps track of the attenuation order and allows 'absorbed' photons to be subtracted from the beam.

VOXEL RESPONSE:

Each voxel that is 'excited' produces a fluorescence response based on a number of factors including dose level and beam intensity.

From elementary physics and unit analysis, the total number of photons passing through a voxel of side-length $A^{1/2}$ is given by [11,12]:

$$\Phi = \left(\frac{\lambda}{hc} \right) (I)(A)(t)$$

Using the Beer-Lambert Law, the fraction of impingent photons absorbed by the FAM molecules within a voxel is given by:

$$\gamma = 1 - e^{-\left(\frac{[C]N_A}{1000}\sigma_{FAM}\right)\sqrt{V}}$$

Where $\sigma_{FAM} = 2.09152 \cdot 10^{-16} \text{ cm}^2$ for a $0.5 \mu\text{M}$ solution.

Using the empirically-determined linear correlation between broken DNA concentration and absorbed radiation ($M = 2.7 \cdot 10^{-3} \mu\text{M}$ SSBs per Gy at $[C] = 0.5 \mu\text{M}$), and assuming that the statistics of photon absorption/emission evenly distributes the photons among active absorbers/emitters, the number of re-emitted stokes-shifted photons can be determined:

number of absorbed photons $\equiv \alpha$

$$\therefore \alpha = \gamma\Phi$$

number of emitted photons $\equiv \varepsilon$

$$\varepsilon = \left(\frac{\text{SSBs}}{\text{Total \# of DNA Strands}}\right) (\text{fluorescence quantum efficiency})(\alpha)$$

$$\therefore \varepsilon = \left(\frac{M}{[C]}\right) (\text{dose})(Q_{FAM})(\alpha)$$

Where $Q_{FAM} = 0.7$ for at $\text{pH} \sim 7$ (i.e. a gelatine phantom solution)

Note: The coded algorithm also allows the effects of photobleaching to be accounted for, based on the probability of damage per excitation. This functionality will not be discussed further, but remains available for use in investigating the trade-off between beam intensity and reconstruction quality.

PHOTON ESCAPE:

Based on the number of emitted fluorescence photons from each excited voxel, this module computes the total number of photons that reach each detector after taking geometric cross-sections and signal attenuation into account. The previously-generated lookup tables are used.

DETECTOR RESPONSE:

An output voltage level is produced based on the specific characteristics of the chosen PMT and control voltage. A more sophisticated model incorporating specific nonlinearities, noise levels and statistical fluctuations was intended, but was not completed due to time constraints. The measured 'Radon Transform' is constructed based on the voltage level for each increment of angle (θ) and planar position (s).

IMAGE RECONSTRUCTION:

This module emulates the actual post-processing required by the readout apparatus to reconstruct the dose profile from the measured detector outputs. To do this, it first applies a digital filter to the raw Radon Transform to remove the radial convolution (i.e. blurring) that is inherent in a pure back-projection. It then converts the filtered Radon Transform to image space using nearest-neighbour interpolation.

*Note: the reconstructed images are normalized based on the maximum FE pixel value. To obtain output values that precisely correspond to dose level (in Grays) would require an empirical calibration scheme. This should be straightforward, but is not discussed in the present work.

5. POST-PROCESSING OPTIMIZATION & RESULTS

Digital filter design is an important factor in reconstruction quality. A raw back-projection tends to ‘oversample’ voxels near the centre of the image, resulting in a blurred reconstruction. In terms of digital filtering, this is equivalent to a “1/R” convolution – where ‘R’ represents the distance from the image centre [11,12]. Correcting this effect requires the oversampling to be ‘inversed’ by adjusting the frequency spectrum of the Radon Transform. To achieve this, the fluorescence variation at each beam position (“S”) and incremental angle (“θ”) is transferred to the frequency domain using a one-dimensional discrete Fourier Transform (DFT). The frequency spectrum is then modulated with an envelope called a filter function before being returned to the spatial domain by an inverse DFT.

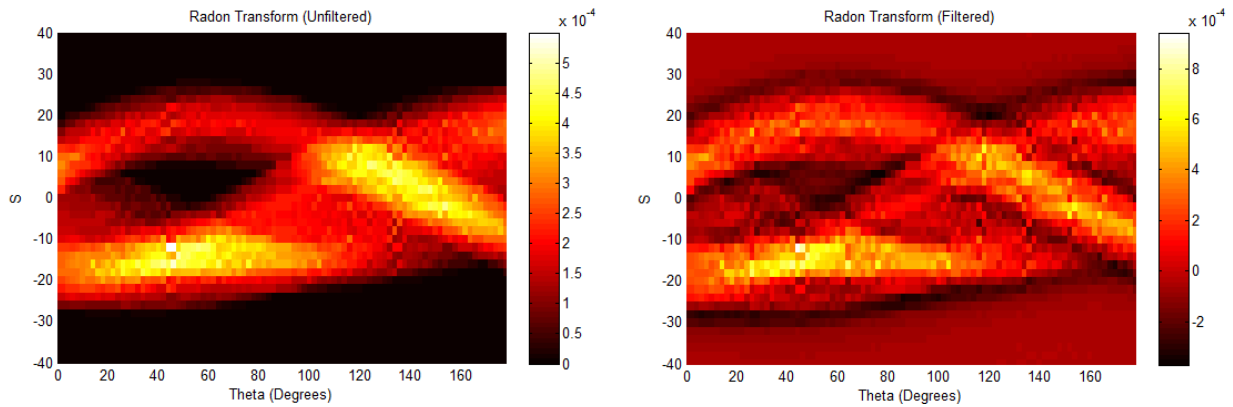


Figure 19 – An example of a Radon Transform before (left) and after (right) digital filtering.

The most mathematically obvious filter for correcting the (1/R) convolution is a ramp function of the form $H(\omega) = \pi|\omega|$, where ω refers to the frequency [11,12]. In practice, however, this filter function introduces unwanted artefacts into the reconstruction image. A custom filter function was designed to address this, with the help of the MATLAB simulation. The optimal solution was found to be a modified “Shepp-Logan” filter of the following form:

$$H(\omega) = \left\{ \begin{array}{l} 0.1 \text{ if } |\omega| \leq \frac{0.01}{2\pi} \\ \pi^2 |\omega| \text{sinc} \left(\frac{\omega}{\omega_{max}} \right) \text{ otherwise} \end{array} \right\}$$

The impact of different filtering schemes on the final reconstruction is illustrated in Figure 20.

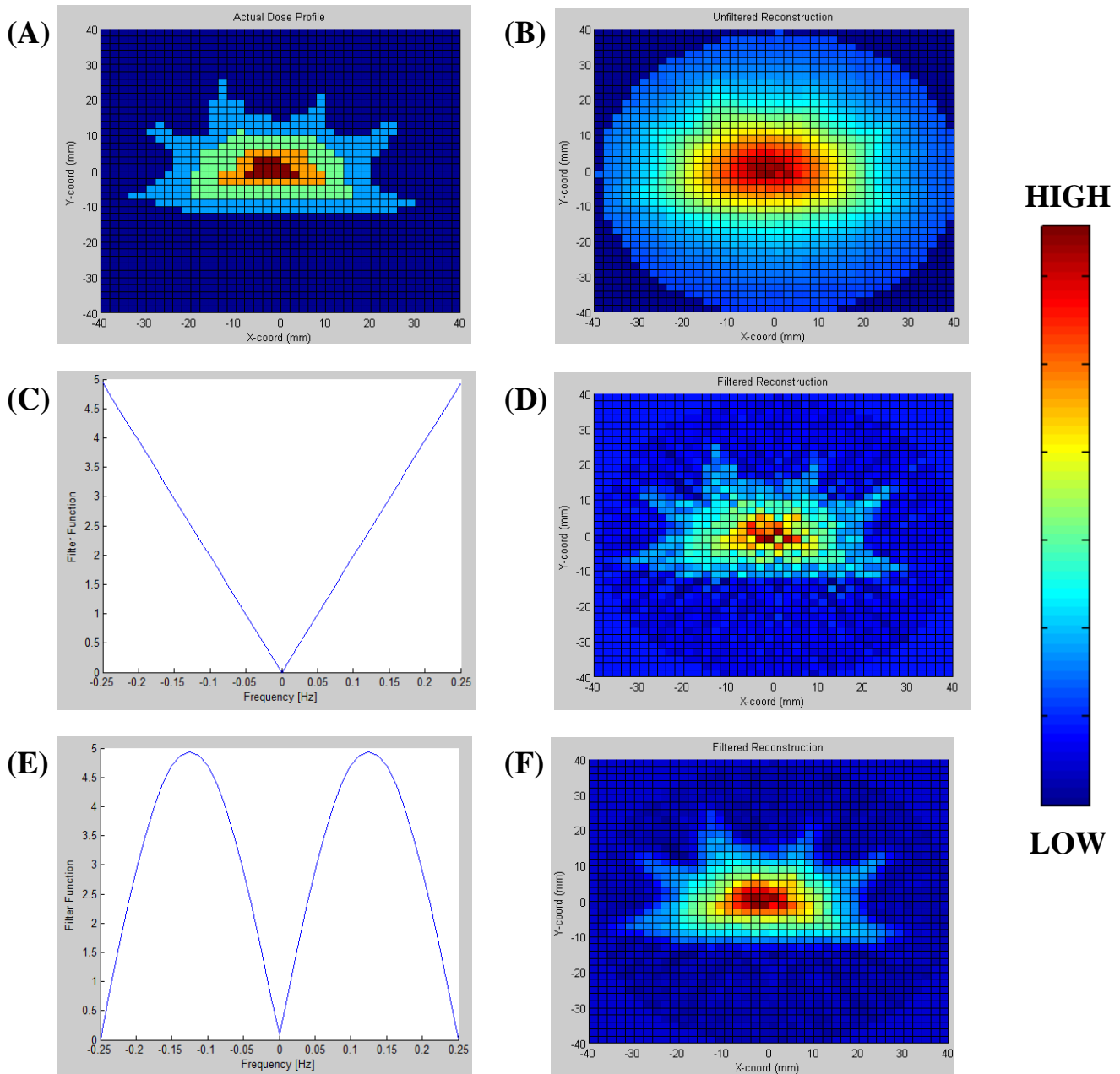


Figure 20 – The effect of digital filtering on dose reconstruction:

- (A) shows a map of the true 2D dose distribution, which resembles a common 7-beam treatment for prostate cancer.
 - (B) depicts the unfiltered CT reconstruction of (A).
 - (C) depicts a ramp-type filter function.
 - (D) shows a reconstruction that has been digitally filtered with the ramp function shown in (C).
 - (E) depicts the optimized filter based on a modified Shepp-Logan function.
 - (F) shows a reconstruction that has been digitally filtered with the function shown in (F).
- All colour scales are relative normalizations of the dose intensity.

The simulation permits exploration of several other design parameters. In reconstructions modelled using the R943-02 Hamamatsu PMT (51 mm diameter), there tends to be additional blurring near the centre of the image as opposed to the larger R1513 PMT (127 mm diameter). This evidences the extent to which detector cross-sections impact the reconstruction quality as shown in Figure 21 below. In contrast, contrary to expectations it was found that the attenuation of fluorescence photons by the BHQ and gelatine molecules in the phantom had negligible impact.

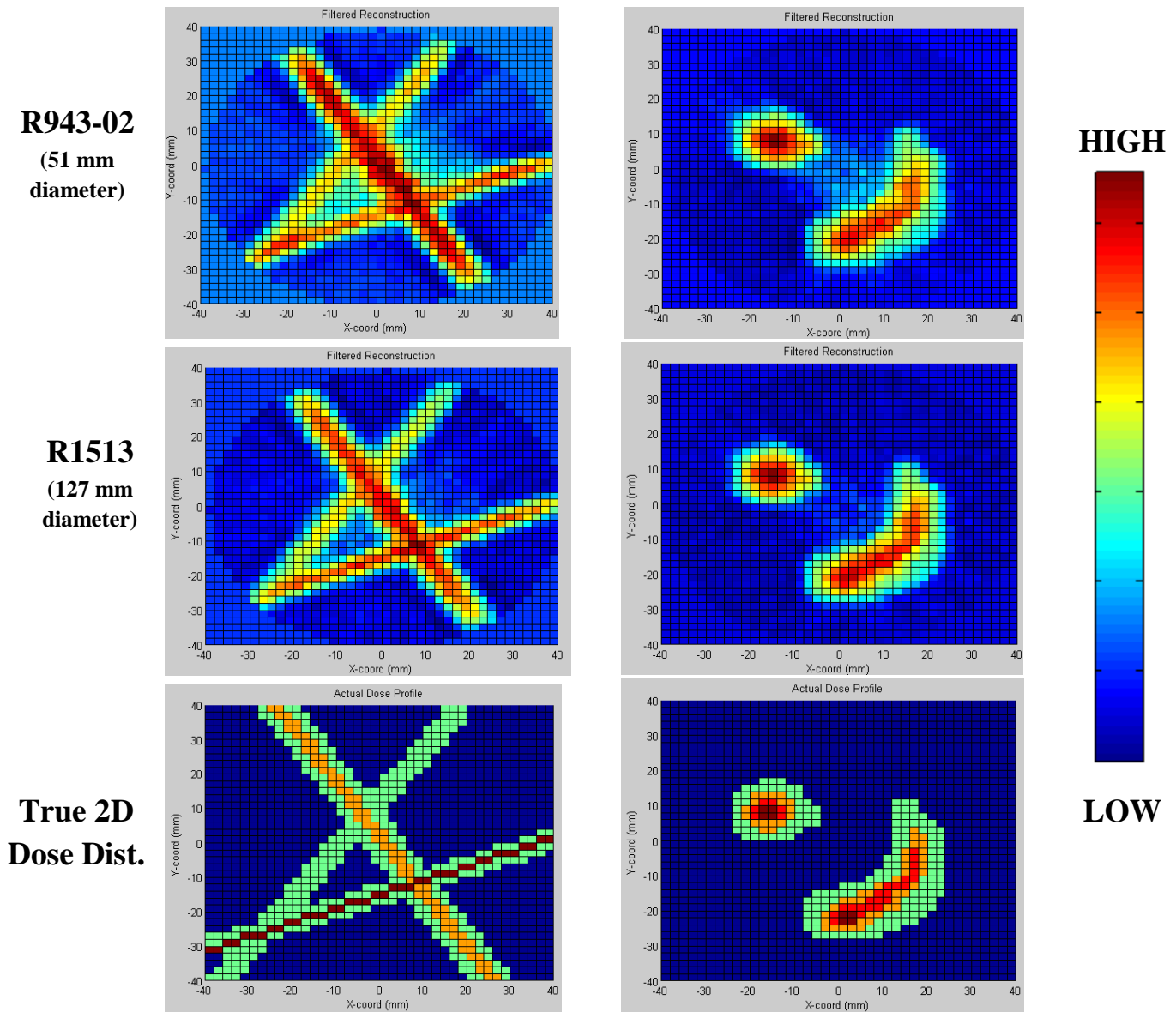


Figure 21 – Performance comparisons between the 51 mm R943-02 PMT (top row), the 127 mm R1513 PMT (central row) and the true 2D dose distribution (bottom row) for two arbitrary dose patterns. The optimized filter function was used. All colour scales are relative normalizations of the dose intensity.

Figure 22 provides an indication of the accuracy to which reconstruction is achieved. Dose distributions were normalized such that a value of 1 was assigned to the highest dose level. The error represents the difference between the normalized doses at each pixel. Most of the higher dose features have an absolute error that is less than 0.15 on the normalized scale. This is reasonably low, but could use significant improvement. The largest errors occur in regions of steep dose gradient (i.e. sharp transitions), which suggests that the majority of these errors may be attributable to slight spatial imprecision inherent in the reconstruction.

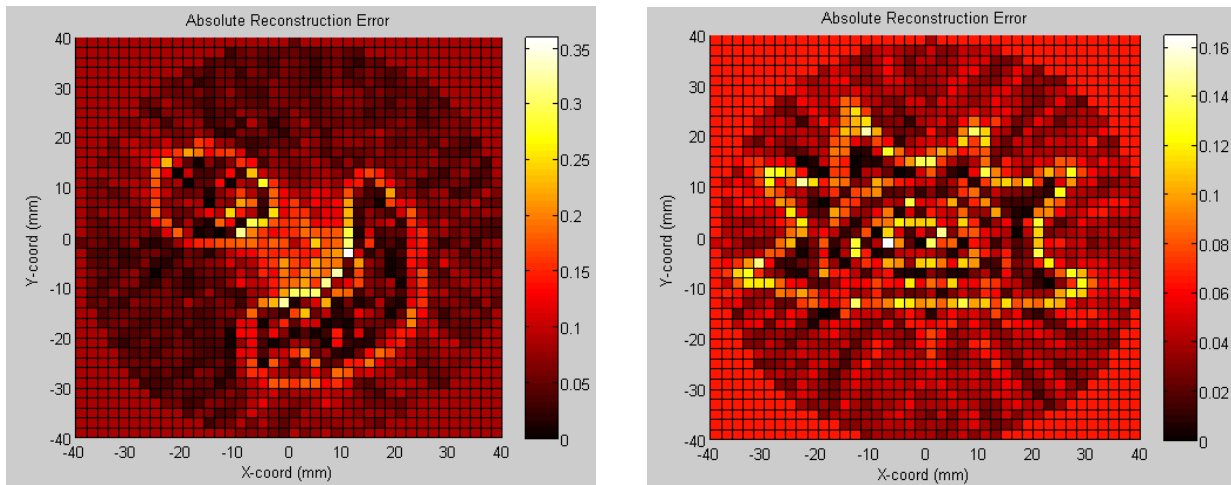
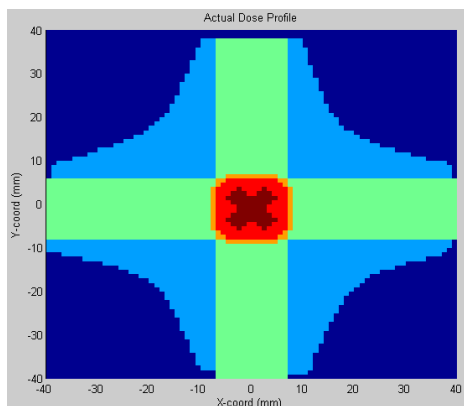


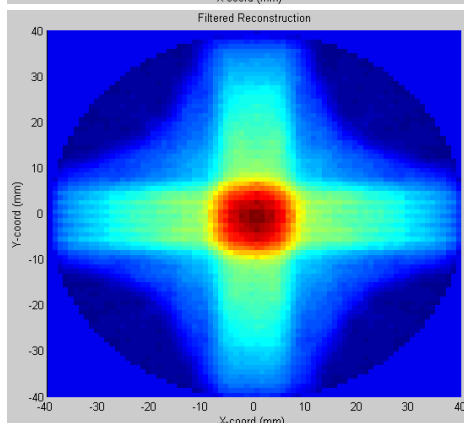
Figure 22 – Error maps depicting the normalized absolute error between a true dose profile and its corresponding reconstruction. The image on the left is for a reconstruction of the dose profile shown at the bottom of the second column in Figure 21. The image on the right originates from the dose pattern featured in Figure 20(A).

While the reconstruction results generally look quite promising, it is clear that a correctional algorithm is necessary to account for the spatial variations in detector cross-section. The highest dose intensities suffer from an inwards ‘smudging’. Sometimes these effects are manageable, as is the case for the reconstructions in Figure 21. Elsewhere they are far too severe. Figure 23 shows some results for a common dose pattern known as the 4-field “box” – fields equally weighted at gantry angles of 0, 90, 180 and 270 degrees. Using the larger PMT improves the situation but does not solve the underlying problem.

**True 2D
Dose Dist.**

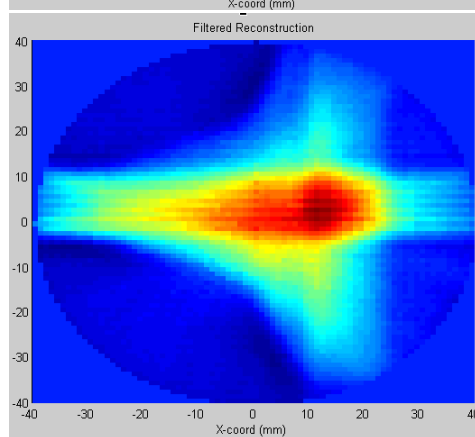
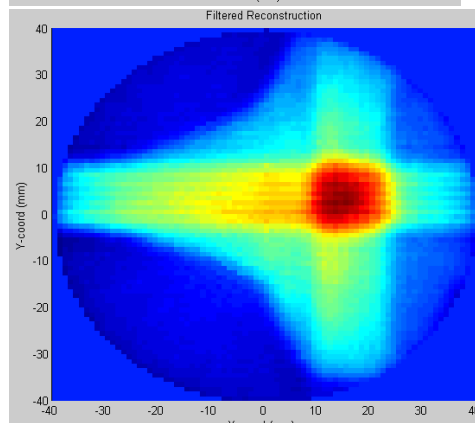
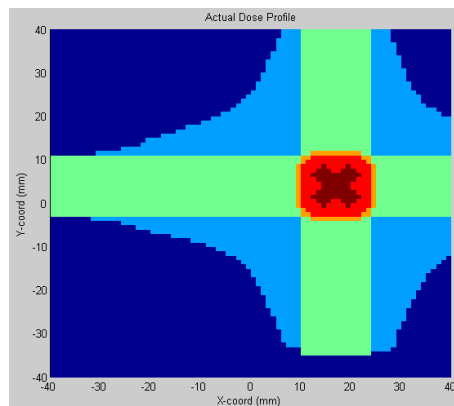


**R1513
(127 mm
diameter)**



**R943-02
(51 mm
diameter)**

“Smudge” effect
becomes more
pronounced for
smaller detector
cross-sections.



HIGH



LOW

Figure 23 – Comparative results for a 4-field box pattern that is centred (left column) versus offset (right column). The inwards smudging effect is most pronounced at high dose intensities, and clearly worsens when a smaller PMT is used, suggesting an intimate relation with the optical geometry.

NOTE: The simulation resolution was increased beyond the intended 2 mm² design resolution.

6. CONCLUSIONS & RECOMMENDATIONS

The findings of this thesis indicate that DNA-based dosimetry is indeed amenable to CT techniques. The reconstruction quality does not match the capabilities of more mature dosimetry platforms; however, what has been achieved thus-far appears promising, considering that this is the first time such functionality has been demonstrated with DNA. It is therefore recommended that this work be continued.

Reconstruction time may prove to be one of the biggest disadvantages of this technique, as the proposed scheme requires an estimated 2.8 hours of measurement time to reconstruct an 8cm diameter, 10cm long phantom whereas many optical dosimeters can produce these results within 10 to 20 minutes [5]. Decreasing the necessary scan time would come at a cost of reconstruction quality.

Significant improvements could be made to the post-processing algorithm to account for the confounding effects of variable detector cross-sections. This might be achieved by multiplying the fluorescence response by a weighting function that depends on beam position. The shortcomings of the present scheme cause an inward radial smudging that greatly distorts features near the periphery of the phantom.

If attempts at finding such a correction are successful, then in principle this CT technique should be on par with the spatial resolutions enjoyed by more established dosimeters. Following this, attempts could be made to refine the dose sensitivity by re-examining several parameters including beam intensity, PMT type, and photon-counting techniques. The computational model should then be improved to better-encapsulate statistical effects, such as variations in the Stokes-shifted wavelengths of the fluorescence photons and the statistics of PMT response.

7. REFERENCES

- [1] Levitt S. H. , Purdy J. A. et al. **Technical Basics of Radiation Therapy – Practical Clinical Applications**. Ed 4, *Springer Publishing*, Berlin (2008).
- [2] Conversations with Dr. Andrew T. Kerr, Senior Medical Physicist at the Cancer Centre of Southeastern Ontario (CCSEO), Kingston, ON, Canada. September 2011 – April 2012.
- [3] Whittum D. H. **Microwave Electron Linacs for Oncology**, in *Reviews of Accelerator Science & Technology*. *World Scientific Publishing Co.*, Vol 2 (2009), pp. 63-92.
- [4] **Radiation Oncology: ‘Clinac’ Treatment Delivery**. *Varian Medical Systems*, accessible at http://www.varian.com/us/oncology/radiation_oncology/clinac/
- [5] Olding T. R. **Cone Beam Optical Computed Tomography-Based Gel Dosimetry**. PhD Dissertation, Queen’s University, Kingston, ON, Canada (2010).
- [6] Mohammadi M., Bezak E., Reich P. **Comparison of two-dimensional transmitted dose maps: evaluation of existing algorithms**. *Australasian Physical & Engineering Sciences in Medicine*, Vol 29, No 2 (2006).
- [7] Wood T., Lewis B.J., et al. **Use of a Dual-Labelled Oligonucleotide as a DNA Dosimeter for Radiological Exposure Detection**. *Radiation Protection Dosimetry* (2011), pp. 1-14.
- [8] E-mail correspondence with Tara Wood, October 13th 2011.
- [9] Förster T. **Intermolecular energy transference and fluorescence**. *Ann. Physik*, Vol 2 (1948), pp. 55-75.
- [10] Email correspondence with Tara Wood, October 24th 2011.
- [11] Hsieh J. **Computed Tomography: Principles, Design, Artefacts and Recent Advances**. *Society of Photo-Optical Instrumentation Engineers*, Washington (2003), pp. 19-73.
- [12] Buzug T. M. **Computed Tomography: From Photon Statistics to Modern Cone-Beam CT**. *Springer*, Berlin (2008), pp. 31-46, 151-183.
- [13] Cong A. X., Wang G. **A finite-element-based reconstruction method for 3D fluorescence tomography**. *Optics Express*, Vol 12, No 24 (2005), pp. 9847-9857.
- [14] Feldkamp L. A., Davic L. C., Kres J. W. **Practical cone-beam algorithm**. *J. Opt. Soc. Am. A*, Vol 1, No 6 (1984), pp. 612-619.
- [15] Bilenca A., Ozcan A. et al. **Fluorescence coherence tomography**. *Optics Express*, Vol 14, No 16 (2006), pp. 7134-7143.

- [16] Freiberger, M. **Nonlinear reconstruction schemes and experimental design for fluorescence diffusion optical tomography**. PhD Dissertation, Technische Universität Graz, Styria, Austria (2010).
- [17] Conversation with Dr. Timothy Olding, Cancer Centre of Southeastern Ontario, November 18th 2011.
- [18] Email correspondence with Tara Wood, November 17th 2012.
- [19] **Opto-semiconductor Handbook**. *Hamamatsu Photonics K. K.* (2011). Available online at http://jp.hamamatsu.com/products/sensor-ssd/index_en.html.
- [20] Taylor S. A. **CCD and CMOS Imaging Array Technologies**. *Xerox Research Centre Europe*, Cambridge, UK (1998). Available online at <http://research.microsoft.com/pubs/80353/ccd.pdf>
- [21] **Photomultiplier Tubes: Basics and Applications**. *Hamamatsu Photonics K. K.*, Ed. 3 (2006). Available online at http://sales.hamamatsu.com/assets/applications/ETD/pmt_handbook_complete.pdf
- [22] **Hitachi Cameras for Industrial Applications** (Product Listing). *Phase 1 Technology Corporation*. Available online at <http://www.phase1tech.com/hitachi-cameras.htm>
- [23] **Avalanche Photodiodes** (Product Listing). *Digikey Corporation*. Available online via www.digikey.ca (Part # SD197-70-72-591-ND).
- [24] **Photomultiplier Tube R1513** (Product Information). *Hamamatsu Photonics K. K.* Available online at <http://sales.hamamatsu.com/en/products/electron-tube-division/detectors/photomultiplier-tubes/part-r1513.php>
- [25] **Photomultiplier Tube R943-02** (Product Information). *Hamamatsu Photonics K. K.* Available online at <http://sales.hamamatsu.com/en/products/electron-tube-division/detectors/photomultiplier-tubes/part-r943-02.php>
- [26] **Photon Counting Using Photomultiplier Tubes**. *Hamamatsu Photonics K. K.* (2005). Available online at http://sales.hamamatsu.com/assets/applications/ETD/PhotonCounting_TPHO9001E04.pdf
- [27] **PMT Module H11526-110-NF** (Product Information). *Hamamatsu Photonics K. K.* Available online at <http://sales.hamamatsu.com/en/products/electron-tube-division/detectors/photomultiplier-modules/part-h11526-110-nf.php>
- [28] **496 nm blocking edge BrightLine long-pass filter** (Product Information). *Semrock (IDEX Corp.)*. Available online at <http://www.semrock.com/FilterDetails.aspx?id=FF01-496/LP-25>

- [29] **Dual-Labelled Probe** (Product Information). *Biosearch Technologies*. Available online at <http://www.boisearchtech.com/store> (Catalog # DLO-FB1-1).
- [30] **Programmable Logic Controllers** (Product Listing). *Automation Direct*. Available online at <http://www.automationdirect.com/static/catalog/index.html>.
- [31] **LTC 2208 16-Bit 130 Msps ADC** (Product Information). *Linear Technologies*. Available online at <http://www.linear.com/purchase/LTC2208>.
- [32] **Solid State Argon Lasers** (Product Information). *Laser Innovations*. Available online at <http://www.laserinnovations.com/448nm.htm>.
- [33] Rothe, R.E. **The Solid Angle at a Point Subtended by a Circle**. *Journal of the Franklin Institute*, Vol 287, No 6 (1969), pp. 515-521.

8. APPENDICES

The following is a transcript of the MATLAB code used to numerically model the CT design.

```
function [ g , gf, svar,thetavar,U, V, InCircle,input_dose_level] = ScanMaster(
dose_img, theta_step, s_step, plot_toggle)
%(C) 2012, Ryan Marchildon

%dose_img is a greyscale image file, created with "ExtractDoseData.m",
%which is an NxN matrix where each pixel has a magnitude corresponding to
%the dose intensity (greater magnitude = greater dose). The number of pixels
%comprising this image will automatically define the grid size of the
%simulation.

[Num, ~] = size(dose_img);

%to translate this into an actual dose value in Greys, an internal metric
%is defined immediately below:

%-----INTERNALLY SET VARIABLES-----
metric = 100;% <- internally user-defined; subject to change!

%LASER PARAMETERS
beam_width = 2; %defines width of excitation laser beam in mm
I = 10; %defines excitation beam intensity in Watts
T = 16*10^(-6); %defines total excitation time per (s,theta) in seconds

%GEOMETRIC PARAMETERS
D = 80; %phantom jar diameter, in mm
l = 55; %distance from centre of phantom to centre of detectors, in mm
Q = D/2;

%PHOTON DETECTOR PARAMETERS
R = 63.5; %radius of photon detectors, in mm
PMT_QE = 0.10; %average PMT Quantum Efficiency at wavelengths of interest
PMT_gain = 3.3E5; %total cathode-to-anode charge amplification
AmpCapacitor = 10^(-9); %1 nF capacitance

%DNA PARAMETERS
DNA_concentration = 0.5; %DNA concentration in phantom, micro Molars
DNA_concentration = DNA_concentration*10^(-6); %convert to mol/L
DNA_FAM_MA = 54700; %defines Molar Absorptivity Coefficient[1/(M*cM)]
DNA_FAM_CS = 3.82*10^(-21)*DNA_FAM_MA; %defines Cross-Section [cm^2]

%ATTENUATION PARAMETERS
mu_phant = 0.15; %<- temporary! 0.15 cm^-1 good estimate (T Olding)
mu_tank = 0; %<- probably a good approximation
%-----

%plot_toggle is a logical 1 or 0, 1 meaning that figures will be shown
%realtime during reconstruction at a cost of computing spend.
```

```

if (plot_toggle ~= 0 && plot_toggle ~= 1)
    error('plot_toggle must be logical 1 or 0');
end

%-----SIMULATION SETUP-----
for (n = 1:1:Num)
    for(m = 1:1:Num)

        %note: readout from image file is in type: int, so if we try to
        %divide by the metric it will round to the nearest integer. We must
        %convert the number to a floating point first!
        input_dose_level(n,m) = double(dose_img(n,m))/metric; %now in Gy
    end
end

%Now set up the coordinate system attached to the dose profile
%U corresponds to X coordinates, V corresponds to Y coordinates
[ cell_length , U, V, InCircle] = GridGen2D( D, Num );

%initialize photobleach matrix
[~,numtemp] = size(U);
photobleach(1:numtemp,1:numtemp) = 0;

%initialize RECONSTRUCTION MATRIX (for animation):
g(1:numtemp,1:numtemp) = 0;

%initialize Fourier-space reconstruction array=====
num_theta = 0;
for (theta=0:theta_step:180-theta_step)
    num_theta = num_theta + 1;
end
theta_tot = num_theta;

num_s = 0;
for (s=(-D/2):s_step:(D/2))
    num_s = num_s + 1;
end
s_tot = num_s;

%=====

%initialize animated figures:
scrsz = get(0,'ScreenSize');
if (plot_toggle == 1)
    fig_laser = figure('Color','white','Toolbar','none','Position',[scrsz(3)/100
    scrsz(4)/1.9 scrsz(3)/2.1 scrsz(4)/2.2]);
    fig_recon = figure('Color','white','Toolbar','none','Position',[scrsz(3)/1.95
    scrsz(4)/1.9 scrsz(3)/2.1 scrsz(4)/2.2]);
    fig_radon = figure('Color','white','Toolbar','none','Position',[scrsz(3)/100
    scrsz(4)/23 scrsz(3)/2.1 scrsz(4)/2.2]);
    fig_orig = figure('Color','white','Toolbar','none','Position',[scrsz(3)/1.95
    scrsz(4)/23 scrsz(3)/2.1 scrsz(4)/2.2]);
end

if (plot_toggle == 1)
    figure(fig_orig);
    hold on

```

```

pcolor(U,V,input_dose_level + InCircle);
xlabel('X-coord (mm)')
shading faceted
%shading interp
ylabel('Y-coord (mm)')
xlim([U(1,1), U(numtemp,numtemp)])
ylim([V(numtemp,numtemp), V(1,1)])
title('Original Input Dose Profile')
hold off
end

%-----

%*****CREATE TABLES FOR NUMERICAL INTEGRATIONS*****
[ fract_top_table,fract_bott_table,
L_Tot_Top_table,L_Phant_Top_table,L_Tot_Bott_table,L_Phant_Bott_table ] = Lookup_Gen(
l,R,Q, U, V, InCircle );
%*****

%*****PRIMARY LOOP*****
%*****
%It is now necessary to perform the scan of the phantom 'slice' by
%translating the beam across the phantom for different angular intervals up
%to 180 degrees.

%theta_step defines the angular step size (in degrees!!!!)
%s_step defines planar sweep step size in millimeters
%d_tol effectively defines the beam width (2*d_tol = w)
d_tol = 0.5*beam_width;

%re-initialize theta and s indices:
num_theta = 0;
num_s = 0;

%SETUP PROGRESS BAR=====
num_bar_counts = 0;

for (theta=0:theta_step:180-theta_step)
    num_bar_counts = num_bar_counts + 1;
end

bar1_step = 1/num_bar_counts;

pbar1 = waitbar(0,'Computing Reconstruction...');

increment_1 = 0; %initialize increment for pbar1
%=====

%Initialize other Misc Variables:
svar(1:s_tot) = (D/2):(-1)*s_step:(-D/2);
thetavar(1:theta_tot) = 0:theta_step:180-theta_step;
F(1:s_tot,1:theta_tot) = 0;

for (theta=0:theta_step:180-theta_step)

```

```

%increase theta count:
num_theta = num_theta + 1;

%Reset figures to speed up processing time (confirmed, reason unknown)
if(plot_toggle == 1)
close(fig_laser);
close(fig_recon);
fig_laser = figure('Color','white','Toolbar','none','Position',[scrsz(3)/100
scrsz(4)/1.9 scrsz(3)/2.1 scrsz(4)/2.2]);
fig_recon = figure('Color','white','Toolbar','none','Position',[scrsz(3)/1.95
scrsz(4)/1.9 scrsz(3)/2.1 scrsz(4)/2.2]);
end

%DISPLAY PROGRESS BAR=====
increment_1 = increment_1 + bar1_step;
waitbar(increment_1 - bar1_step,pbar1)
%=====

%Reset S-counter:
num_s = 0;

for (s=(D/2):(-1)*s_step:(-D/2))

%increase s count:
num_s = num_s + 1;

%Simulate the excitation pencil beam
[ Illum, ORDER_n, ORDER_m ] = LaserGen( theta, s, U, V, InCircle, D, d_tol);
%Returns:
% Illum(n,m) - logical: Illuminated? 1=Yes, 0=No
% ORDER_n(p) - p denotes illumination order, gives n-index
% ORDER_m(p) - p denotes illumination order, gives m-index

%-----ANIMATE BEAM PATH-----
%Now plot the grids that were illuminated by the beam, just to
%check that the code is working!

if (plot_toggle == 1)
figure(fig_laser);
hold on
pcolor(U,V,Illum + InCircle);
xlabel('X-coord (mm)')
shading faceted
%shading interp
ylabel('Y-coord (mm)')
xlim([U(1,1), U(numtemp,numtemp)])
ylim([V(numtemp,numtemp), V(1,1)])
title('Visualization of Excitation Beam')
hold off
end
%-----
%pause(0.25) %this pause allows enough time for the animation to be viewed by
the user

%Internal Error Check:

```

```

Num_Illum = length(ORDER_n);

if (Num_Illum ~= length(ORDER_m))
    error('Internal Error!')
end

signal_strength = 0; %reset signal output before looping through this set of
excited cells

%step through each illuminated cell in order of illumination:
for (p=1:1:Num_Illum)

    n = ORDER_n(p);
    m = ORDER_m(p);
    X0 = U(n,m);
    Y0 = V(n,m);
    dose = input_dose_level(n,m); %retrieves the does for the cell

    %simulate the generation of photons at the cell site
    [ alpha,epsilon, photobleach(n,m) ] = photon_gen(
DNA_concentration,DNA_FAM_CS ,cell_length,dose,I,T,photobleach(n,m) );
    %alpha represents the number of photons removed from the beam
    %epsilon is the number of photons released from that point
    %photobleach keeps track of the number of relevent destroyed
    %FAM molecules

    %Now switch coordinate systems so that the detectors are
    %stationary
    [ x_cell,y_cell ] = ToDetector( X0, Y0, theta, s );

    %Determine which grid point these transformed coordinates are
    %closest to so that the lookup tables can be used!
    %=====
    [indtemp2,~] = size(U);

    difftemp2 = 10000000000000000;

    for (n2=1:1:indtemp2);

        difftemp3 = abs(x_cell - U(1,n2));

        if (difftemp3 <= difftemp2)
            xXx = n2; % index of closest X grid match
            difftemp2 = difftemp3;
        end

    end

    difftemp2 = 10000000000000000;

    for (n2=1:1:indtemp2);

        difftemp3 = abs(y_cell - V(n2,1));

        if (difftemp3 <= difftemp2)

```

```

        yYy = n2; % index of closest Y grid match
        difftemp2 = difftemp3;
    end

end

%=====

%ASSUMING NO ATTENUATION...-----
%what percentage of outbound photons make it to Top Detector?
[ fract_top ] = fract_top_table( xXx, yYy );
epsilon_top = epsilon*fract_top; %compute the # of photons

%what percentage of outbound photons make it to Bottom Detector?
[ fract_bott ] = fract_bott_table( xXx, yYy );
epsilon_bott = epsilon*fract_bott; %compute the # of photons
%-----

%HOW MANY PHOTONS ACTUALLY GET ATTENUATED BY OTHER MOLECS?-----
%-----

%For Top Detector...
%what is the average path length to the detector?
L_Tot_Top = L_Tot_Top_table( xXx, yYy );
%what is the average path length through the phantom?
L_Phant_Top = abs(L_Phant_Top_table( xXx, yYy ));
%what is the average path length through the matching tank?
L_Tank_Top = L_Tot_Top - L_Phant_Top;
%attenuation through the phantom:
epsilon_top = epsilon_top*exp((-1)*mu_phant*L_Phant_Top/10);
%attenuation through the matching tank:
epsilon_top = epsilon_top*exp((-1)*mu_tank*L_Tank_Top/10);
%now epsilon_top represents the # of photons that actually
%reach the top detector!

%For Bottom Detector...
%what is the average path length to the detector?
L_Tot_Bott = L_Tot_Bott_table( xXx, yYy );
%what is the average path length through the phantom?
L_Phant_Bott = abs(L_Phant_Bott_table( xXx, yYy ));
%what is the average path length through the matching tank?
L_Tank_Bott = L_Tot_Bott - L_Phant_Bott;
%attenuation through the phantom:
epsilon_bott = epsilon_bott*exp((-1)*mu_phant*L_Phant_Bott/10);
%attenuation through the matching tank:
epsilon_bott = epsilon_bott*exp((-1)*mu_tank*L_Tank_Bott/10);
%now epsilon_bott represents the # of photons that actually
%reach the bottom detector!
%-----

%-----DETECTOR MODULE-----
%Can later simulate the nonlinearities of the detector (PMT)

```

```

%Top Detector:
Nelec_Top = PMT_QE*epsilon_top; %how many photoelectrons made?
AnodeCharge_Top = (1.6E-19)*PMT_gain*Nelec_Top; %charge at Anode
Vout_Top = AnodeCharge_Top/AmpCapacitor; %magnitude of Vout

%Bottom Detector:
Nelec_Bott = PMT_QE*epsilon_bott; %how many photoelectrons made?
AnodeCharge_Bott = (1.6E-19)*PMT_gain*Nelec_Bott; %charge at Anode
Vout_Bott = AnodeCharge_Bott/AmpCapacitor; %magnitude of Vout

%This model assumes the use of an integrating charge amplifier
%-----

%-----CONVERSION MODULE-----
%This simulates further amplification, introduction of noise,
%ADC to computer interface, etc.

%NOTE***PROGRAMMING ABANDONED DUE TO TIME CONSTRAINTS***
signal_strength = signal_strength + Vout_Top + Vout_Bott;
%signal strength will continue to build up as the response of
%each excited cell is totalled.
%-----
%add data to reconstruction matrix

end

%now assign cumulative signal strength value to the excited line
for (p=1:1:Num_Illum)
    n = ORDER_n(p);
    m = ORDER_m(p);
    g(n,m) = g(n,m) + signal_strength;
end

%construct F(theta,s)
F(num_s,num_theta) = signal_strength;

%*****ANIMATE RECONSTRUCTION*****
if (plot_toggle == 1)
figure(fig_recon)
hold on
pcolor(U,V,g);
xlabel('X-coord (mm)')
shading faceted
%shading interp
ylabel('Y-coord (mm)')
xlim([U(1,1), U(numtemp,numtemp)])
ylim([V(numtemp,numtemp), V(1,1)])
title('Raw Reconstruction (Unfiltered)')
hold off
end
%*****

%pause(0.25)

```

```

end

%*****ANIMATE RADON TRANSFORM*****
if (plot_toggle == 1)
figure(fig_radon)
hold on
imagesc(thetavar,svar,F);
xlabel('Theta (Degrees)')
colormap(hot)
colorbar
ylabel('S')
ylim([svar(s_tot), svar(1)])
xlim([thetavar(1), thetavar(theta_tot)])
title('Radon Transform (Unfiltered)')
hold off
end
%*****

%close %closes previous figure... speeds up laser animation! (why?)

end

close(pbar1) %close progress bar

if (plot_toggle == 1)
close(fig_radon)
close(fig_laser)
close(fig_orig)
end

%*****
%*****

%=====POST-PROCESSING RECONSTRUCTION=====

%Apply Digital Filter and Map Back to Image Space
[ g,FF,gf ] = ImageFilter( F , svar,thetavar,U, V, InCircle,input_dose_level );

%Quality-Assurance
fig_g = figure('Color','white','Toolbar','none','Position',[scrsz(3)/100 scrsz(4)/1.9
scrsz(3)/2.1 scrsz(4)/2.2]);
fig_gf = figure('Color','white','Toolbar','none','Position',[scrsz(3)/100 scrsz(4)/1.9
scrsz(3)/2.1 scrsz(4)/2.2]);
fig_Orig = figure('Color','white','Toolbar','none','Position',[scrsz(3)/1.95
scrsz(4)/1.9 scrsz(3)/2.1 scrsz(4)/2.2]);
fig_radon = figure('Color','white','Toolbar','none','Position',[scrsz(3)/100
scrsz(4)/23 scrsz(3)/2.1 scrsz(4)/2.2]);
fig_radonF = figure('Color','white','Toolbar','none','Position',[scrsz(3)/1.95
scrsz(4)/23 scrsz(3)/2.1 scrsz(4)/2.2]);

N = numtemp;

figure(fig_Orig);

```

```

hold on
pcolor(U,V,input_dose_level);
xlabel('X-coord (mm)')
shading faceted
ylabel('Y-coord (mm)')
xlim([U(1,1), U(N,N)])
ylim([V(N,N), V(1,1)])
title('Actual Dose Profile')
hold off

figure(fig_g);
hold on
pcolor(U,V,g);
xlabel('X-coord (mm)')
shading faceted
ylabel('Y-coord (mm)')
xlim([U(1,1), U(N,N)])
ylim([V(N,N), V(1,1)])
title('Unfiltered Reconstruction')
hold off

figure(fig_gf);
hold on
pcolor(U,V,gf);
xlabel('X-coord (mm)')
shading faceted
ylabel('Y-coord (mm)')
xlim([U(1,1), U(N,N)])
ylim([V(N,N), V(1,1)])
title('Filtered Reconstruction')
hold off

figure(fig_radon)
hold on
imagesc(thetavar,svar,F);
xlabel('Theta (Degrees)')
colormap(hot)
colorbar
ylabel('S')
ylim([svar(s_tot), svar(1)])
xlim([thetavar(1), thetavar(theta_tot)])
title('Radon Transform (Unfiltered)')
hold off

figure(fig_radonF)
hold on
imagesc(thetavar,svar,FF);
xlabel('Theta (Degrees)')
colormap(hot)
colorbar
ylabel('S')
ylim([svar(s_tot), svar(1)])
xlim([thetavar(1), thetavar(theta_tot)])
title('Radon Transform (Filtered)')
hold off

%=====

end

```

```

function [ cell_length , U, V, InCircle] = GridGen2D( D, Num )
%(C) Ryan Marchildon, Nov 17th, 2011

%This function will generate a 2D grid of elements to represent a slice
%through the dosimeter 'phantom'. Each grid element will be labelled with a
%particular index. Note, all cells/elements are taken to be square.

%INPUT ARGUMENTS:
%D = Desired phantom Diameter (mm)
%Num (N) = Number of element divisions along diameter
%   -MUST BE AN ODD NUMBER!

%Run Initialization Check on Input Parameters:-----
if(mod(Num,2) == 0)
    error('N must be an ODD integer')
elseif(mod(Num,2) ~= 1)
    error('N must be an odd INTEGER')
end
%-----

%Calculate Cell Length:
cell_length = D/(Num-1);

%Generate Element Indexes and Coordinates
%   -Start by making a square grid
%NOTE: indexes cannot be negative, unfortunately... list positive indexes
%first, then beyond N - (N-1)/2, go to negative numbers.
%BUT: What I will do here is just start from the TOP LH corner
%because I don't know what indexing difficulties to anticipate for the
%actual image reconstruction

xmin = ((-1)*(Num-1)*cell_length) + cell_length/2;
xmax = ((1)*(Num-1)*cell_length) - cell_length/2;
ymin = ((-1)*(Num-1)*cell_length) + cell_length/2;
ymax = ((1)*(Num-1)*cell_length) - cell_length/2;

for (n=1:1:Num) %cycle through rows

    for (m=1:1:Num) %cycle through columns

        %Matrix for All X Coordinates
        U(n,m) = (-1)*((Num-1)/2)*cell_length + cell_length*((m-1) );
        %Matrix for all Y Coordinates
        V(n,m) = ((Num-1)/2)*cell_length - cell_length*((n-1) );

        %Determine which elements are within the circle:
        Mag(n,m) = sqrt((norm(U(n,m)))^2 + (norm(V(n,m)))^2);

        if ( Mag(n,m) <= (D/2))
            InCircle(n,m) = 1;
        elseif (Mag(n,m) > (D/2))
            InCircle(n,m) = 0;
        end

    end

end

end

```

```

%REMEMBER - these squares are NOT the actual cells
%rather, the plotted POINTS represent the centre of the cells
end

%*****
%*****
%*****

function [ fract_top_table,fract_bott_table,
L_Tot_Top_table,L_Phant_Top_table,L_Tot_Bott_table,L_Phant_Bott_table ] = Lookup_Gen(
l,R,Q, U, V, InCircle )
%This function creates 'lookup tables' of numerical integrations to save
%computing time. All excitation points will be approximated to sites on the
%mesh.

[N,~] = size(U);

%Initialize the 'look-up' tables:

fract_top_table(1:N,1:N) = 0;

fract_bott_table(1:N,1:N) = 0;

L_Tot_Top_table(1:N,1:N) = 0;

L_Phant_Top_table(1:N,1:N) = 0;

L_Tot_Bott_table(1:N,1:N) = 0;

L_Phant_Bott_table(1:N,1:N) = 0;

%SETUP PROGRESS BAR=====
num_bar_counts = N;

bar1_step = 1/num_bar_counts;

pbar1 = waitbar(0,'Forming Integral Tables...');

increment_1 = 0; %initialize increment for pbar1
%=====

for (n=1:1:N)

%DISPLAY PROGRESS BAR=====
increment_1 = increment_1 + bar1_step;
waitbar(increment_1 - bar1_step,pbar1)
%=====

for (m=1:1:N)

%Check to see if we need to bother with the computation:
%-----
Yes = 0; %by default do not proceed with calculation

```

```

    if( n >= 2 && m >= 2 && n < N && m < N)

        if (InCircle(n,m) == 1 || InCircle(n-1,m) == 1 || InCircle(n+1,m) == 1 ||
InCircle(n,m-1) == 1 || InCircle(n,m+1) == 1)

            Yes = 1;

        end

    else
        if (InCircle(n,m) == 1)

            Yes = 1;

        end

    end

%-----

if (Yes == 1)

    %Perform the necessary numerical integrations

    x_cell = U(n,m);

    y_cell = V(n,m);

    fract_top_table(n,m) = Cross_Top( l, R, x_cell, y_cell );

    fract_bott_table(n,m) = Cross_Bott( l, R, x_cell, y_cell );

    L_Tot_Top_table(n,m) = L_Total_Top( l,R,x_cell,y_cell );

    L_Phant_Top_table(n,m) = L_P_Top( Q, R, x_cell, y_cell );

    L_Tot_Bott_table(n,m) = L_Total_Bott( l,R,x_cell,y_cell );

    L_Phant_Bott_table(n,m) = L_P_Bott( Q,R,x_cell,y_cell );

end

end

end

close(pbar1);

end

%*****
%*****
%*****

function [ percent_of_flux ] = Cross_Top( l, R, x0, y0 )
%This function computes the total cross-section of the top detector with

```

```

%respect to the outward flux of photons from the excited cell. This
%cross-section is then converted into a percentage of the total outbound
%photon flux.

%l = distance between phantom centre and detector centre
%x0 = horizontal position of excited cell
%y0 = vertical position of excited cell
%R = radius of detector

%Imporant variable definitions:

L = l - y0;
theta = atan(abs(x0)/L);
r = sqrt(L^2 + (abs(x0))^2);
lambda = r/R;

%initialize index
n = 0;

%initialize step size
steps = 1000;
stepsize = (2*pi)/steps;

%itialize arrays to save computation time
f(1:steps) = 0;
x(1:steps) = 0;

for (phi=0:stepsize:2*pi)

    n = n + 1;

    %The function we want to integrate over:
    f(n) = ((lambda-sin(theta)*cos(phi))/(1-((sin(theta))^2)*((cos(phi))^2)))*(1 -
(2*lambda*sin(theta)*cos(phi))/(1 + lambda^2));
    x(n) = phi;

end

%compute integral numerically using the Trapezoidal Rule
integral = trapz(x,f);

%compute cross-section
OMEGA = 2*pi - cos(theta)*((1 + lambda^2)^(-1/2))*integral;

%convert cross-section to a fraction of the spherical flux
percent_of_flux = OMEGA/(4*pi);

end

%*****
%*****
%*****

function [ percent_of_flux ] = Cross_Bott( l, R, x0, y0 )
%This function computes the total cross-section of the bottom detector with

```

```

%respect to the outward flux of photons from the excited cell. This
%cross-section is then converted into a percentage of the total outbound
%photon flux.

%l = distance between phantom centre and detector centre
%x0 = horizontal position of excited cell
%y0 = vertical position of excited cell
%R = radius of detector

%Imporant variable definitions:

L = l + y0;
theta = atan(abs(x0)/L);
r = sqrt(L^2 + (abs(x0))^2);
lambda = r/R;

%initialize index
n = 0;

%initialize step size
steps = 1000;
stepsize = (2*pi)/steps;

%itialize arrays to save computation time
f(1:steps) = 0;
x(1:steps) = 0;

for (phi=0:stepsize:2*pi)

    n = n + 1;

    %The function we want to integrate over:
    f(n) = ((lambda-sin(theta)*cos(phi))/(1-((sin(theta))^2)*((cos(phi))^2)))*(1 -
(2*lambda*sin(theta)*cos(phi))/(1 + lambda^2));
    x(n) = phi;

end

%compute integral numerically using the Trapezoidal Rule
integral = trapz(x,f);

%compute cross-section
OMEGA = 2*pi - cos(theta)*((1 + lambda^2)^(-1/2))*integral;

%convert cross-section to a fraction of the spherical flux
percent_of_flux = OMEGA/(4*pi);

end

%*****
%*****
%*****

function [ int_value ] = L_P_Top( Q, R, x0, y0 )
%This function performs the numerical integration to compute the average
%path length taken from the photon source to the "top" detector.

```

```

%need to specify R,x0,y0,Q
%Q is the radius of the Phantom dosimeter jar
%R is the radius of the circular detector face
%x0,y0 are the coordinates of the excited cell
%l is the distance between the phantom centre and the detector centre

%PS in MATLAB the function log(X) takes the NATURAL (not base 10) logarithm

n = 0; %initialize index

stepsize = 2*R/1000; %want to break computation into 1000 steps;

steps = 2*R/stepsize; %calc # of steps to initialize array

f(1:steps) = 0; %initialize array

for (x=(-1)*R:stepsize:R)

    n = n + 1;

    C = (x-x0)^2 + (sqrt(Q^2 - x^2)-y0)^2;

    f(n) = sqrt(R^2-x^2)*sqrt(C+R^2-x^2)-(1/2)*C*log(-sqrt(R^2-x^2)+sqrt(C+R^2-x^2))+(1/2)*C*log(sqrt(R^2-x^2)+sqrt(C+R^2-x^2));

    %fix potential issues with obtaining log(0) in the second term
    g(n) = -sqrt(R^2-x^2)+sqrt(C+R^2-x^2);
    if(g(n) == 0)
        f(n) = f(n-1);
    end

    X(n) = x;

end

int_value = trapz(X,f); %sum of all possible path lengths
int_value = int_value/(pi*R^2); %normalize the output

end

%*****
%*****
%*****

function [ int_value ] = L_P_Bott( Q,R,x0,y0 )
%This function performs the numerical integration to compute the average
%path length taken from the photon source to the "top" detector.

%need to specify R,x0,y0,Q
%Q is the radius of the Phantom dosimeter jar
%R is the radius of the circular detector face
%x0,y0 are the coordinates of the excited cell

```

```

%PS in MATLAB the function log(X) takes the NATURAL (not base 10) logarithm

n = 0; %initialize index

stepsize = 2*R/1000; %want to break computation into 1000 steps;

steps = 2*R/stepsize; %calc # of steps to initialize array

f(1:steps) = 0; %initialize array

for (x=(-1)*R:stepsize:R)

    n = n + 1;

    C = (x-x0)^2 + ((-1)*sqrt(Q^2 - x^2)-y0)^2; %only diff. from 'top' alg.

    f(n) = sqrt(R^2-x^2)*sqrt(C+R^2-x^2)-(1/2)*C*log(-sqrt(R^2-x^2)+sqrt(C+R^2-x^2))+(1/2)*C*log(sqrt(R^2-x^2)+sqrt(C+R^2-x^2));

    %fix potential issues with obtaining log(0) in the second term
    g(n) = -sqrt(R^2-x^2)+sqrt(C+R^2-x^2);
    if(g(n) == 0)
        f(n) = f(n-1);
    end

    X(n) = x;

end

int_value = trapz(X,f); %sum of all possible path lengths
int_value = int_value/(pi*R^2); %normalize the output

%Note: computation was tested and found to be accurate to ~0.005% within the
%vicinity of (x0,y0) = (0,0)

end

%*****
%*****
%*****

function [ int_value ] = L_Phantom_Top( Q, R, x0, y0 )
%This function performs the numerical integration to compute the average
%path length taken from the photon source to the "top" detector.

%need to specify R,x0,y0,Q
%Q is the radius of the Phantom dosimeter jar
%R is the radius of the circular detector face
%x0,y0 are the coordinates of the excited cell
%l is the distance between the phantom centre and the detector centre

%PS in MATLAB the function log(X) takes the NATURAL (not base 10) logarithm

n = 0; %initialize index

```

```

stepsize = 2*R/1000; %want to break computation into 1000 steps;

steps = 2*R/stepsize; %calc # of steps to initialize array

f(1:steps) = 0; %initialize array

for (x=(-1)*R:stepsize:R)

    n = n + 1;

    C = (x-x0)^2 + (sqrt(Q^2 - x^2)-y0)^2;

    f(n) = sqrt(R^2-x^2)*sqrt(C+R^2-x^2)-(1/2)*C*log(-sqrt(R^2-x^2)+sqrt(C+R^2-
x^2))+(1/2)*C*log(sqrt(R^2-x^2)+sqrt(C+R^2-x^2));

    X(n) = x;

end

int_value = trapz(X,f); %sum of all possible path lengths
int_value = int_value/(pi*R^2); %normalize the output

end

%*****
%*****
%*****

function [ int_value ] = L_Phantom_Bott( Q,R,x0,y0 )
%This function performs the numerical integration to compute the average
%path length taken from the photon source to the "top" detector.

%need to specify R,x0,y0,l
%Q is the radius of the Phantom dosimeter jar
%R is the radius of the circular detector face
%x0,y0 are the coordinates of the excited cell
%l is the distance between the phantom centre and the detector centre

%PS in MATLAB the function log(X) takes the NATURAL (not base 10) logarithm

n = 0; %initialize index

stepsize = 2*R/1000; %want to break computation into 1000 steps;

steps = 2*R/stepsize; %calc # of steps to initialize array

f(1:steps) = 0; %initialize array

for (x=(-1)*R:stepsize:R)

    n = n + 1;

    C = (x-x0)^2 + ((-1)*sqrt(Q^2 - x^2)-y0)^2; %only diff. from 'top' alg.

    f(n) = sqrt(R^2-x^2)*sqrt(C+R^2-x^2)-(1/2)*C*log(-sqrt(R^2-x^2)+sqrt(C+R^2-
x^2))+(1/2)*C*log(sqrt(R^2-x^2)+sqrt(C+R^2-x^2));

```

```

    X(n) = x;

end

int_value = trapz(X,f); %sum of all possible path lengths
int_value = int_value/(pi*R^2); %normalize the output

%Note: computation was tested and found to be accurate to ~0.005% within the
%vicinity of (x0,y0) = (0,0)

end

%*****
%*****
%*****

function [ int_value ] = L_Total_Top( l,R,x0,y0 )
%This function performs the numerical integration to compute the average
%path length taken from the photon source to the "top" detector.

%need to specify R,x0,y0,l

%PS in MATLAB the function log(X) takes the NATURAL (not base 10) logarithm

n = 0; %initialize index

stepsize = 2*R/1000; %want to break computation into 1000 steps;

steps = 2*R/stepsize; %calc # of steps to initialize array

f(1:steps) = 0; %initialize array

for (x=(-1)*R:stepsize:R)

    n = n + 1;

    C = (x-x0)^2 + (l-y0)^2;

    f(n) = sqrt(R^2-x^2)*sqrt(C+R^2-x^2)-(1/2)*C*log(-sqrt(R^2-x^2)+sqrt(C+R^2-
x^2))+(1/2)*C*log(sqrt(R^2-x^2)+sqrt(C+R^2-x^2));

    X(n) = x;

end

int_value = trapz(X,f); %sum of all possible path lengths
int_value = int_value/(pi*R^2); %normalize the output

end

%*****
%*****
%*****

function [ int_value ] = L_Total_Bott( l,R,x0,y0 )
%This function performs the numerical integration to compute the average
%path length taken from the photon source to the "top" detector.

```

```

%need to specify R,x0,y0,l

%PS in MATLAB the function log(X) takes the NATURAL (not base 10) logarithm

l = (-1)*1; % <- only difference from top detector algorithm

n = 0; %initialize index

stepsize = 2*R/1000; %want to break computation into 1000 steps;

steps = 2*R/stepsize; %calc # of steps to initialize array

f(1:steps) = 0; %initialize array

for (x=(-1)*R:stepsize:R)

    n = n + 1;

    C = (x-x0)^2 + (l-y0)^2;

    f(n) = sqrt(R^2-x^2)*sqrt(C+R^2-x^2)-(1/2)*C*log(-sqrt(R^2-x^2)+sqrt(C+R^2-x^2))+
(1/2)*C*log(sqrt(R^2-x^2)+sqrt(C+R^2-x^2));

    X(n) = x;

end

int_value = trapz(X,f); %sum of all possible path lengths
int_value = int_value/(pi*R^2); %normalize the output

end

%*****
%*****
%*****

function [ Illum, ORDER_n, ORDER_m ] = LaserGen( theta, s, U, V, InCircle, D, d_tol)
%This function generates a virtual laser beam at a particular orientation.
%The angle from the x-axis is defined by theta. For any given theta the
%beam can then be moved across a plane by translating through a range -s to
%+s. The objective is to determine which grid points are 'illuminated' by
%the beam.

%THETA MUST BE IN Degrees!!!
%Convert Theta to radians now:
theta = pi/180*theta;

%U is a matrix containing the x-coordinate data for every grid point, as
%generated by GridGen2D

%V is a matrix containing the y-coordinate data for every grid point, as
%generated by GridGen2D

%InCircle is a true/false matrix indicating whether the coordine falls
%within the phantom dosimeter jar (i.e. "In the circle")

```

```

%D is the diameter of the phantom that was used to define the grid in
%GridGen2D

%d_tol is the maximum distance from the laser beam at which a gridpoint
%will be considered 'illuminated' ---- basically, it is related to the
%chosen beam width!

%NOTE! Can save calculation time later by only doing computation for
%gridpoints that lie within the phantom jar circle (i.e. incircle matrix
%from GridGen2D)

%*****BEAM TRACING & ILLUMINATION*****
%Determine number of rows and columns in grid space:
[N,N] = size(U);

if (size(U) ~= size(V))
    error('U and V matrices are not equal size!')
end

%Define distance of beam source from grid centre
r = (D/2)*sqrt(2);

%Define location of beam source as well as mirror pair:
x1 = r*cos(theta);
y1 = r*sin(theta);
x2 = (-1)*x1;
y2 = (-1)*y1;

%Make modifications to shift beam according to "s" parameter:
deltaX = -s*sin(theta);
deltaY = s*cos(theta);
x1 = x1 + deltaX;
x2 = x2 + deltaX;
y1 = y1 + deltaY;
y2 = y2 + deltaY;

%Now define line that traces out beam path:
if (y1==y2)
    CASE = 1; % case where slope = 0
elseif (abs(x1 - x2) <= 10^(-3))
    CASE = 2; % case where slope = infinity
else
    CASE = 0;
    slope = (y1-y2)/(x1-x2);
    b = y1 - slope*x1;
end

%Now loop through each gridpoint and determine how close it is to beam and
%therefore whether or not it becomes illuminated by laser light

%Pre-Allocate memory for illumination matrix:

```

```

Illum(1:N,1:N) = 0;

for (n=1:1:N)
    for (m=1:1:N)

        %Only do the calculation for gridpoints "InCircle"
        if (InCircle(n,m) == 1)

            x0 = U(n,m);
            y0 = V(n,m);

            if (CASE == 0) %nonzero finite slope

                %Define intersecting line (y = -1/m*x + c)
                %Note: this characterizes shortest d from gridpoint to beam

                c = y0 + (1/slope)*x0;

                %Find point of intersection

                xint = (c-b)/(slope+1/slope);
                yint = slope*xint + b;

                %Calculate shortest distance between gridpoint and beam

                d = sqrt((x0-xint)^2 + (y0-yint)^2);

            elseif (CASE == 1) %zero slope

                d = sqrt((y0 - y1)^2);

            elseif (CASE == 2) %infinite slope (undefined)

                d = sqrt((x0 - x1)^2);

            end

            %Now logical statement: illuminated? Yes or No

            if (d <= d_tol)
                Illum(n,m) = 1;
            else
                Illum(n,m) = 0;
            end

        end

    end

end

end
%*****

```

```

%*****ILLUMINATION ORDER*****
%Now wish to calculate an 'illumination order' for the purpose of
%determining beam attenuation later on...

distance(1:N,1:N) = 0; %initialize array to save computing time
num = 0; %a placeholder to index the ACTIVE point number

for (n=1:1:N)
    for (m=1:1:N)
        %Only do the calculation for Illuminated Gridpoints
        if (Illum(n,m) == 1)

            %Calculate distance from laser source
            distance(n,m) = sqrt((U(n,m) - x1)^2 + (V(n,m) - y1)^2);

            %add nonzero illum count to total number of illuminated cells:
            num = num+1;

        end
    end
end

Z = num; %define total number of illuminated points that we must search
count_index_n(1:Z) = 0; %initialize count indices
count_index_m(1:Z) = 0;
count_index_dist(1:Z) = 0;

%now build up the entire count index:

index = 0; %re-initialize new index number

for (n=1:1:N)
    for (m=1:1:N)
        %Only index Illuminated Gridpoints
        if (Illum(n,m) == 1)

            index = index + 1;
            count_index_n(index) = n;
            count_index_m(index) = m;
            count_index_dist(index) = distance(n,m);

        end
    end
end

%now sort through count index to create an order for the gridpoints (n,m)
%based upon illumination order (i.e. smallest distance to largest)

[~,s_indices] = sort(count_index_dist); %default sorts in ascending order
%note: first entry would be re-ordered array, second entry is index

%initialize new arrays to save computing time:
ORDER_n(1:Z) = 0;
ORDER_m(1:Z) = 0;

for (p = 1:1:Z)

```

```

        index = s_indices(p);
        ORDER_n(p) = count_index_n(index);
        ORDER_m(p) = count_index_m(index);

end
%*****

end

%*****
%*****
%*****

function [ x_cell,y_cell ] = ToDetector( X0, Y0, theta, s )
%Performs Coordinate transform in preparation for computing the number of
%photons that make it to each detector

%X0,Y0 is the coordinate of the excited cell in the phantom's frame of
%reference (i.e. the laser and detectors rotate around a stationary
%phantom)

%THETA MUST BE IN Degrees!!!
%Convert Theta to radians now:
theta = pi/180*theta;

%*****COORDINATE TRANSFORM 1*****
%Transform the coordinate of the excited cell into the frame in which the
%phantom rotates but the laser and detectors are stationary

%Use the definition of the rotation matrix to find the new coordinate:

x_cell = cos(theta)*X0 + sin(theta)*Y0;
y_cell = (-1)*sin(theta)*X0 + cos(theta)*Y0;

%PS: checked the output! transform appears to be working properly!
%*****

end

%*****
%*****
%*****

function [ alpha,epsilon, bleached_DNA ] = photon_gen(
conc,sigma,cell_length,dose,I,T,photobleach )
%This function simulates the cell response to the excitation beam. It first
%calculates the number of photons absorbed by the FAM molecules, and then
%determines the number of stokes-shifted photons that are re-emitted. It is
%assumed that these photons are emitted in any direction with equal
%probability (i.e. uniformly distributed throughout a spherical flux).

%conc = concentration of DNA moles
%sigma = absorption cross-section of FAM moles
%I = incident laser intensity, W/m^2
%T = amount of time pulse is active, s
%dose = amount of delivered dose in Grays
%photobleach = number representing the number of photobleached moles
bleached_DNA = photobleach;

```

```

%Declare physical constants:
cell_length = cell_length/1000; %convert cell length from mm to m
A = cell_length^2;
h = 6.626*10^(-34); % m^2kg/s - Planck's Constant
c = 299792458; %m/s - Speed of Light in Vacuum
lambda = 488*10^(-9); %m - peak absorption wavelength for FAM
Na = 6.022*10^23; % Avogadro's number
M = 0.0054; %linear coefficient in broken DNA vs delivered dose relation
bleach_probability = 0; %arbitrarily assigned

%compute total number of broken DNA strands:
brkn_DNA = 0.0054*dose*conc*Na*cell_length^3/1000;

%compute number of photons absorbed:
alpha = (lambda/(h*c))*I*T*A*(1 - exp(-(conc*Na/1000)*sigma*cell_length/100));

if (brkn_DNA ~= 0)
%compute the number of photons re-emitted:
epsilon = M*dose*0.7*alpha*(1- bleached_DNA/brkn_DNA);
%note: 0.7 represents overall quantum efficiency
%the last term accounts for the photobleaching effect
else
    epsilon = 0;
end

%how many relevent molecs were destroyed by photobleaching?
new_bleach = M*dose*alpha*bleach_probability;

%add this to the photobleached total:

bleached_DNA = bleached_DNA + new_bleach;

end

%*****
%*****
%*****

function [ g,FF,gf ] = ImageFilter( F , svar,thetavar,U, V, InCircle,input_dose_level
)
%This function is used for experimenting with different filter parameters

theta_tot = length(thetavar);
s_tot = length(svar);
s_step = abs(svar(2) - svar(1));

c1 = 1;
c2 = pi;

%=====POST-PROCESSING RECONSTRUCTION=====

%PART I: Apply Filtering to the Radon Transform (i.e. projections)
%*****
[NNN,~] = size(F);
for (thetaind=1:1:theta_tot)

```

```

Y1 = fft(F(1:NNN,thetaind))/NNN; %take discrete Fourier transform
Y1 = fftshift(Y1); %center frequencies about f = 0

freq = (-NNN/2 + 0.5):1:(NNN/2 - 0.5); %generate associated frequencies
freq = freq/(s_step*(NNN-1)); %apply proper scaling

freqmax = freq(length(freq)); %magnitude of max frequency used

%NOW ACT UPON FT WITH FILTER KERNAL
for (n=1:1:length(freq))

    if (abs(freq(n)) <= 0.01)
        H(n) = 0.1;
        Y2(n) = Y1(n)*H(n);
    else
        H(n) = c1*pi*abs(2*pi*freq(n))*(sinc(freq(n)*c2/(pi*freqmax))*pi);
        %H(n) = pi*abs(2*pi*freq(n)); %ramp filter
        Y2(n) = Y1(n)*H(n);
    end
end

Y3 = ifftshift(Y2); %shift back to original DFT output
Y3 = ifft(Y3*NNN); %take inverse Fourier transform

FF(1:NNN,thetaind) = Y3(1:NNN); %assign filtered Radon Transform

end

%PART II: Convert to Image Space (using nearest-neighbour interpolation)
%*****

[N,M] = size(U);

if (N ~= M)
    error('Houston, we have a problem');
end

ss(1:N,1:N) = 0; % initialize interpolation matrix
g(1:N,1:N) = 0; % reconstruction matrix (unfiltered)
gf(1:N,1:N) = 0; % reconstruction matrix (filtered)

for (thetaind=1:1:theta_tot)

    %compute s-value for each (x,y) for this given angle
    for (n=1:1:N)
        for (m=1:1:M)
            if (InCircle(n,m) ==1)
                %compute "s" for that gridpoint (remember to convert to
                %radians)
                ss(n,m) = U(n,m)*cos(pi/180*thetavar(thetaind)) +
V(n,m)*sin(pi/180*thetavar(thetaind));
            else
                ss(n,m) = 10000000; %assign out of range value
            end
        end
    end
end
end

```

```

    for (sind=1:1:s_tot)
        for(n=1:1:N)
            for(m=1:1:M)
                if(abs(ss(n,m) - svar(sind)) <= 1) %see if pixel matches s
                    g(n,m) = g(n,m) + F(sind,thetaind);
                    gf(n,m) = gf(n,m) + FF(sind,thetaind);
                end
            end
        end
    end

end

%normalize g by number of contributing angles:
g = g/theta_tot;
gf = gf/theta_tot;

%For some reason this algorithm rotates the image by 90 degrees CW
%Thus the output matrices must be rotated by 90 degrees CCW to compensate
g = rot90(g);
gf = rot90(gf);
%=====
end

```

CODE FOR ERROR EVALUATION:

```

function [ input,gf_output, error_map, max_error ] = ErrorMap( U,V,input_dose_level,
gf )
% gf = dose distribution as measured by the CT algorithm
% input_dose_level = true dose distribution
% U -> x coordinates for image
% V -> y coordinates for image

[N,M] = size(U);

%=====
%Normalize both dose distributions with respect to the largest dose
%magnitude found in either array, such that the highest intensity
%corresponds to an element value of 1.

%make sure no values are negative:*****

%initialize values:
present_min_gf = 100000000000;

%run loop
for (n = 1:1:N)
    for(m = 1:1:M)
        value = gf(n,m);
        if (value <= present_min_gf)
            present_min_gf = value;
        end
    end
end
end

```

```

correction = (-1)*present_min_gf;
gf = gf + correction;

%search for the max value:*****

%initialize values:
present_max_gf = -100000000000;

%run loop
for (n = 1:1:N)
    for(m = 1:1:M)
        value = gf(n,m);
        if (value >= present_max_gf)
            present_max_gf = value;
            index_n_gf = n;
            index_m_gf = m;
        end
    end
end

if (present_max_gf == 0)
    error('Something went horribly, horribly wrong');
end

gf = gf/present_max_gf; %normalize!

%check normalization:
if (gf(index_n_gf,index_m_gf) ~= 1)
    error('Something went horribly, horribly wrong');
end

%make sure no values are negative:*****

%initialize values:
present_min_input = 100000000000;

%run loop
for (n = 1:1:N)
    for(m = 1:1:M)
        value = input_dose_level(n,m);
        if (value <= present_min_input)
            present_min_input = value;
        end
    end
end

correction = (-1)*present_min_input;
input_dose_level = input_dose_level + correction;

%search for the max value:*****

%initialize values:
present_max_input = -100000000000;

```

```

%run loop
for (n = 1:1:N)
    for(m = 1:1:M)
        value = input_dose_level(n,m);
        if (value >= present_max_input)
            present_max_input = value;
            index_n_input = n;
            index_m_input = m;
        end
    end
end

if (present_max_input == 0)
    error('Something went horribly, horribly wrong');
end

input = input_dose_level/present_max_input; %normalize!

%check normalization:
if (input(index_n_input,index_m_input) ~= 1)
    error('Something went horribly, horribly wrong');
end

%=====

%       figure();
%       hold on
%       pcolor(U,V,gf);
%       xlabel('X-coord (mm)')
%       shading faceted
%       ylabel('Y-coord (mm)')
%       xlim([U(1,1), U(N,N)])
%       ylim([V(N,N), V(1,1)])
%       title('gf after')
%       hold off

%=====
%Compute the error (with respect to the true dose) for each pixel

error_map(1:N,1:N) = 0 ;

for (n = 1:1:N)
    for(m = 1:1:M)
        error_map(n,m) = abs(gf(n,m) - input(n,m));
    end
end

percent_map(1:N,1:N) = 0 ;

for (n = 1:1:N)
    for(m = 1:1:M)
        if (gf(n,m) == 0)
            percent_map(n,m) = abs(gf(n,m) - input(n,m))/0.000000001;
        else
            percent_map(n,m) = abs(gf(n,m) - input(n,m))/gf(n,m);
        end
    end
end

%correct background in percent map:

```

```

for (n = 1:1:N)
    for(m = 1:1:M)
        if (percent_map(n,m) == 1)
            percent_map(n,m) = 0;
        end
    end
end

%Determine the Max error:*****

%initialize values:
max_error = 0;

%run loop
for (n = 1:1:N)
    for(m = 1:1:M)
        value = error_map(n,m);
        if (value >= max_error)
            max_error = value;
        end
    end
end

%Plot the Error Map

figure()
hold on
pcolor(U,V,error_map);
colormap(hot)
colorbar
xlabel('X-coord (mm)')
ylabel('Y-coord (mm)')
xlim([U(1,1), U(N,N)])
ylim([V(N,N), V(1,1)])
title('Absolute Reconstruction Error')
hold off

%Plot the % Error Map

figure()
hold on
pcolor(U,V,100*percent_map);
colormap(hot)
colorbar
xlabel('X-coord (mm)')
ylabel('Y-coord (mm)')
xlim([U(1,1), U(N,N)])
ylim([V(N,N), V(1,1)])
title('% Reconstruction Error')
hold off

%=====

gf_output = gf;

end

```